ORIGINAL PAPER

Improving the Co-removal Efficiency of Dyes from Water by a Novel Four-Component Chitosan Flexible Film Containing Graphene Oxide

Saed Salami[1] · Morteza Bahram[1] · Khalil Farhadi[1] · Legha Ansari[2]

Abstract

In the present study, a quaternary composite consisting of α-ketoglutaric acid, chitosan, polyaniline, and graphene oxide (α-CTS-PANI-GO) was synthesized and characterized by Scanning Electron Microscope, Fourier Transform Infrared Spectroscopy, and Raman spectroscopy. The adsorption of dye on the film was proved by the X-ray diffraction analysis method. According to the increase in the intensity of the peak before and after adsorption, it showed the presence of Methylene Blue (MB) and Acid Orange 7 (AO7). Also, the appearance of peaks related to sulfur in Energy dispersive X-ray (EDX) and EDX elemental mapping, and X-ray photoelectron spectroscopy data after the adsorption process proved the presence of dyes compounds and their adsorption by the synthetic film. The simultaneous removal properties of α-CTS-PANI-GO were evaluated in the removal of cationic and anionic dyes, MB and AO7. Using the Central Composite Decomposition, the effect of different variables such as pH, temperature, adsorbent dose, and time on AO7 and MB removal was studied. The regeneration of α-CTS-PANI-GO film was studied and the zero point charge of the synthesized film was also determined. Various isotherm models, such as Langmuir and Freundlich, were investigated, and the processing of experimental equilibrium data confirmed the suitability and application of the Langmuir model. Analysis of experimental adsorption data using various kinetic models, such as pseudo-first and second-order models, shows the applicability of the first-order equation. The results showed that in the optimal conditions, the removal percentage was about 95% for AO7 and 80% for MB, which indicates the successful performance of the synthetic film compared to the method.

Keywords α-Ketoglutaric acid · Chitosan film · Polyaniline · Graphene oxide · Cationic dyes · Anionic dyes

Introduction

One of the major environmental and public problems in the world is water pollution, which has always received significant attention [1] non-availability of clean drinking water is one of the most important health issues in modern times. Industrial dyes are one of the dominant chemicals that make water unfit for drinking [2]. Synthetic dyes are used in different industries and the exact amount of dyes discharged from various industries to the environment are unknown. However, the release of high amounts of dyes to the environment

has posed severe challenges to scientists [3].Industries such as painting, leather, clothing, pulp, paper, textiles, and others use a variety of dyes [4]. In the textile industry, two types of dyes are used to dye fabrics: natural dyes and synthetic dyes. Among the several types of dyes used worldwide, the largest group is azo dyes that have one or more azo bonds (–N=N–) in their structure [5]. AO7 is one of the water-soluble azo dyes which is widely used in paper and textile industries. In fact, during the dyeing bath on the fibers, there are pollutants such as dyes and auxiliary products that are not stabilized in the effluents of industrial paper and textile factories. In the textile industry, among several categories of dyes, azo dyes make up about 60–70% of the dyes used. Some of them, such as AO7, show aquatic toxicity or sensitizing effects, and produce aromatic amines that are carcinogenic under reduced conditions [6]. Carcinogenicity is one of the properties of this dye [7]. MB is one of the large cation dyes that is present in textile wastewater and is discharged into the environment without proper management,

✉ Morteza Bahram
  m.bahram@urmia.ac.ir

1   Department of Analytical Chemistry, Faculty of Chemistry, Urmia University, Urmia, Iran

2   Cellular and Molecular Research Center, Cellular and Molecular Medicine Research Institute, Urmia University of Medical Sciences, Urmia, Iran

especially in developing countries. MB was commonly used for dyeing cotton wool and silk [8]. Methylene blue is one of these organic dyes, known as an organic chloride salt with acidic properties and high toxicity.Also, this organic dye causes respiratory, digestive, and mental disorders [9]. MB is toxic, carcinogenic, and non-biodegradable and can be a serious threat to human health and environmental safety. It is usually released in natural water sources, which becomes a threat to human health and living organisms [2]. High costs, technical problems, and other limitations have prevented many methods, such as ion exchange resins, filtering membranes, electrodialysis, and biologically active methods for dye treatment in industrial wastewater. Therefore, nowadays, there is a need to develop new and more effective decolorization strategies that are environmentally friendly and suitable for industrial use [10]. Different adsorbents have been suggested to remediate aqueous solutions contaminated with organics; These include activated carbon, graphene, zeolites, polymers, metal oxides/hydroxides, waste-derived materials, and porous silica. In the realm of wastewater treatment, Metal–Organic Frameworks (MOFs), characterized by superior porosity, stability, and surface area, have garnered significant attention However, MOFs in powder form present challenges in terms of regeneration. To address this, the creation of membrane materials with fiber strands through electrospinning offers an effective solution. Electrospinning is a facile method for producing fibrous nanofibers with high porosity and a high surface area-to-volume ratio2f [11]. In particular, carbonaceous materials and their composites have been widely utilized owing to their exceptional properties, such as a large specific surface area, abundant pore structure, chemical stability, ease of physical and chemical modification, ability to be tuned for specific applications and their ability to remove a variety of pollutants [12] Carbon nanomaterials (CNMs) have garnered more attention in the water treatment field due to their hollow layered structures, π–π Strong electrostatic interactions and large specific surface areas.1b [13] At the same time, natural polymers such as collagen (COL), silk fibroin (SF), and hyaluronic acid (HA) displayed excellent biocompatibility, high safety, biodegradability, low toxicity, and lower immune resistance.Due to their poor mechanical strength, high surface tension, and poor solubility in organic solvents, it is challenging to fabricate nanofibers from natural polymers; however, they could be combined with synthetic polymers to produce nanofibers with enhanced mechanical strength2.b [14].

Having large amounts of amino and hydroxyl functional groups that can be complexed with pollutants is one of the important characteristics of chitosan (CTS) [15]. Antifungal and antimicrobial activities are other characteristics of this polymer [16]; hence, it is used in the food storage industry, wound healing, and drug delivery systems [17, 18]. Of course, the use of chitosan is limited due to its lack of

strong mechanical properties and its hydrophilic properties [19]. One effective modification is the transformation of the amino group to N-glutaric acid by Schiff base reactions [20]. Therefore, we used α-ketoglutaric acid for modification of CTS to obtain a functional polymer, which contains Schiff-base groups. These kinds of CTS derivatives have powerful complexation ability and great adsorption characteristics.

Due to the interaction of polyaniline (PANI) with organic dyes by electrostatic interactions, hydrogen bonding, and π–π interactions between aromatic parts of organic dyes and polyaniline, the use of polyaniline in removing organic dyes is of great interest. In addition, PANI has good environmental stability. As well, the synthesis of PANI is simple and cheap [21]. According to the literature, CTS and PANI have been used for methylene blue dye removal previously [19]. The removal efficiency of CTS film was only 44% after 16 h, while the CTS/PANI film had a removal efficiency of 98% within 2 h. It is reported that CTS/PANI /Fe$_3$O$_4$ nanocomposite has been applied to the removal of reactive red dye [22]. The results show that the highest removal percentage was 94.25% with a mass ratio of CS/PANI (1:1), and the lowest removal percentage was 86.95% for the mass ratio of CTS/PANI (1:2). Therefore, we tried to maximize the removal of dyes by using PANI in the synthesis process of α-CTS flexible film.

The incorporation of graphene oxide (GO) into the polymer as the water treatment agent is very attractive for many purposes. Two-dimensional structure, the ability to increase negative surface charges, excellent electron transfer, creating a high surface area, harmlessness, and remarkable chemical stability are among its unique properties. Dispersibility in water, flux, surface hydrophilicity, and mechanical resistance are increased by using GO [23]. Due to the structure of (GO), which contains various oxygenated functional groups (for example, carboxyl (-COOH), carbonyl, epoxy (C–O–C), and hydroxyl (–OH) groups), it has negative charges in the sheets. Then, cationic dyes can have strong electrostatic interactions with these groups [24]. Also, GO reveals good biocompatibility [25]. In addition, the preparation of GO is easy and provides the potential for the synthesis of low-cost and large-scale productions. In a study, GO/PANI nanocomposite was used to remove brilliant green (BG) [26]. The adsorption of BG onto GO/PANI nanocomposite had a monolayer adsorption capacity (qm) of 142.8 mg/g. In other study, the preparation of graphene oxide@chitosan (GO@CS) composite beads was investigated via continuous dropping techniques to remove methylene blue (MB)-dye from an aqueous media.The adsorption of MB onto GO@CS composite beads had a maximum adsorption capacities of 23.26 mg/g.1a [27] Accordingly, due to all the aforementioned advantages, most importantly, excellent mechanical strength and excellent cationic dye adsorption, we rationally used GO for the improvement of the α-CTS-PANI film.

In this work, for the first time, we used four materials: α-ketoglutaric acid, chitosan, polyaniline, and graphene oxide for the synthesis of a strong and flexible adsorbent film. After synthesizing the film, we evaluated the ability of dye adsorption by placing it in dye solutions prepared from MB and AO7. We also investigated the changes in the adsorption behavior of the film at different times, pH, and adsorbent concentrations. Moreover, we proved the adsorption properties of the film by different methods such as EDX, XPS, and XRD. According to the obtained results, it was found that all four components of the synthetic film affect the removal mechanism of the dyes. Another advantage of the synthetic film is that it can be easily separated from the solution without using a separation process such as centrifuging. Also, it should be mentioned that this synthetic film is cheap, reusable, easy to synthesize, environmentally friendly, and has high physical resistance. There are no noticeable disadvantages for the adsorbent used.

Materials and Methods

Materials

Alpha-Ketoglutaric Acid (AKA) was purchased from Sigma. Chitosan and aniline monomers were purchased from Dr.Gholami (Iran) and Borhan (Iran), respectively. Acetic acid, graphite powder, sodium nitrate ($NaNO_3$), potassium permanganate, sulfuric acid, sodium borohydride ($NaBH_4$), hydrogen peroxide, and glycerol were purchased from Merck. Hydrochloric acid (Merck) and sodium hydroxide (Merck) were used for the preparation of the solution (0.1 M) for pH adjustment. AO7 (Merck), MB (Merck), 1.5 ppm stock solution of AO7 and MB was prepared by dissolving suitable amounts of dyes in water. Deionized Water was used all over the experiments. All chemicals were used as purchased without further purification.

Synthesis of Polyaniline (PANI)

For this purpose, 50 ml of 1 M hydrochloride was placed in an ice bath, then 0.66 ml of distilled aniline (monomer) was added and stirred for 15 min. Finally, oxidant solution (APS 0.01 (mg/L) dissolved in 1 M HCl) was added to the monomer solution for 30 min under stirring at 0–4 °C. After 4 h, the precipitate was separated from the solution and was washed 3 times with deionized water and dried in air at 70 °C into an oven by 5 h [28].

Synthesis of Graphene Oxide (GO)

The Hummers method was used to synthesize GO. Synthetic graphite powder was purchased from Merck. The

GO synthesis method was as follows: A 500 ml balloon was placed in an ice bath and kept at 5 °C. Graphite (1 g), sodium nitrate ($NaNO_3$, 0.50 g), and concentrated sulfuric acid (H_2SO_4, 23 ml) were added while stirring constantly. After 5 min, potassium permanganate ($KMnO_4$, 3 g) was gently added to the balloon to prevent a severe reaction. The reaction was kept at 5 °C for 2 h, and then the reaction temperature was slowly raised to 35 °C and stirred for another 30 min. Deionized water (DI) (46 ml) was added to the suspension, increasing the temperature of hydration temperature to 98 °C. The reaction was kept at this temperature for 30 min. Then, at the end of the reaction, deionized water (140 ml) and hydrogen peroxide (10% by volume, 10 ml) were added to the balloon. The resulting brown/yellow product was separated from the solution by vacuum filtration. To remove residual manganese ions and acid, the obtained GO powders were washed 5 times with diluted HCl solution (5% 200 ml) and hot deionized water (70 °C) and then were dried at 60 °C in an oven for 12 h [29].

Synthesis of α-CTS-PANI-GO Film

The adsorbent was prepared as follows. In brief, CS (3 g) was dissolved in 10 ml (1 wt%) acetic acid, and alpha-ketoglutaric acid (4 g) was added to the solution and stirred for 24 h at 37 °C. Then sodium borohydride (0.4 g) was added and further stirred for 10 h. Graphene oxide(0.05 g) and polyaniline(0.05 g) were dispersed in a (1 wt%) acetic acid. It was then added to the CS and alpha-ketoglutaric acid and stirred at 120 rpm for 4 h. At the end of the reaction, 10 drops of glycerol were added to the mixture. The prepared (α-CTS-PANI-GO) film was dried in an oven at 50 °C for 24 h.

Characterization of α-CTS-PANI-GO Film

The characterization evaluations were done on the final film, α-CTS-PANI-GO. The FTIR spectra were recorded With a Thermo Nicolet Nexus-670 Fourier transform infrared spectrophotometer (USA). The Raman spectra were recorded using a Thermo Nicolet Almega Dispersive Raman Spectrometer. The morphological studies were carried out by a ZEISS Sigma VP scanning electron microscope (FE-SEM, C26 DME—9550E, DME–SPM Company, Denmark). A PG-Instruments T80 + UV–Vis spectrophotometer was used for recording the absorbance of solutions at selected wavelengths. X-ray diffraction (XRD) patterns of the composites and their components were recorded using GNR APD 2000 PRO X-ray diffractometer, Cu–Kα radiation source was operated at 40 kV and 30 mA in the scanning range of $2\theta = 5$–90° and scan rate of 0.02° s^{-1}. The morphology was examined using JEOL, JSM-6340F. Moreover, measurements were conducted on an ESCALAB Xi + X-ray

photoelectron spectrometer (Thermo Fischer, USA) with an Al Kα X-ray source (hν = 1486.6 eV) as the excitation source and a vacuum pressure of 8×10–10 Pa in the analytical chamber. The pass energy used for the high-resolution scan was 100 eV. it should be noted that all instruments were calibrated. As well we repeated each test at least 3 times.

Synthetic Wastewater Preparation

In the preparation process of the stock solution, 0.05 g of MB ($C_{16}H_{18}N_3SCl$) and AO7 were weighed and added into two different 1 L of Erlenmeyer flasks. After that, distilled water was poured into each flask in the specified amount of 1000 ml, and complete dissolution was performed using a glass stirrer. Then, different working solutions were prepared using the concept of the dilution process. Finally, the two solutions were mixed to obtain the final solution.

Treatment Method

In this study, after the synthesis of the α-CTS-PANI-GO film, solutions with different concentrations of dyes AO7 and MB were prepared. Then, using the experiment design software, various parameters such as temperature, adsorption percentage, and time were checked. 20 ml of dye solution with different amounts of adsorbent were tested at different temperatures and times, and the adsorption percentage at specific wavelengths for each dye was measured before and after adding the adsorbent. To investigate the synergistic effect of different adsorbents was synthesized, and the effect of each factor was investigated.

Theoretical Background

Adsorption Isotherms

To obtain the adsorption isotherm using two common models, Langmuir and Freundlich adsorption isotherms, the experiment was performed using initial concentrations of MB and AO7 (0.5, 1, 1.5, 2, 2.5, and 3 mg/l) at a constant adsorbent dose of 0.004 g, contact time 60 min, and pH 6. The Langmuir isotherm assumes that each adsorption site can adsorb only one species, and adsorption is done monolayer on the surface of the adsorbent. The linear shape of the Langmuir isotherm model is shown in Eq. 1:

$$\frac{1}{q_e} = \frac{1}{q_{max}} + \frac{1}{K_{lqmax}C_e} \tag{1}$$

where q_{max} (mg/g) is the maximum adsorption capacity of the MB and AO7 adsorbed per unit mass of (ACS-P-G) film, K_L (l/mg) is the Langmuir constant, which is related to the equilibrium adsorption constant. C_e (mg/L) is the equilibrium value of MB and AO7 concentration, and q_e (mg/g) is the value of MB and AO7 adsorption capacity. In addition, the constant (R_L) of Langmuir adsorption, which is called the dimensionless constant parameter separation, was measured using Eq. 2:

$$R_L = \frac{1}{1 + K_L C_0} \tag{2}$$

where C_o (mg/L) is the initial MB and AO7 concentration.

The linearized form of the Freundlich isothermal equation used in this study was described using Eq. 3:

$$Log q_e = Log K_f + \frac{1}{n} Log q C_e \tag{3}$$

where K_f [(mg/g) (l/mg)/n] is the Freundlich constant, which represents adsorption capacity, and 'n' (unitless) represents adsorption intensity. Basically, 'n' is used to describe the favorability of the adsorption process [30].

Kinetic Models

The equation of the pseudo-first-order kinetic model is Eq. 4:

$$Log \frac{q_e}{q_e - q_t} = \frac{K_1}{2.303} t \tag{4}$$

where q_e refers to the amount of dye adsorption (mg g^{-1}) at equilibrium, and q_t refers to the the value of dye adsorption (mg g^{-1}) at different times, t (min). The equilibrium rate constant of the pseudo-first-order sorption is k_1 (min^{-1}).

The equation of the pseudo-second-order kinetic model is Eq. 5:

$$\frac{1}{q_e - q_t} = \frac{1}{q_e} + k_2 t \tag{5}$$

where the equilibrium rate constant of the pseudo-second-order adsorption is k_2 (g mg^{-1} min^{-1}). Eq. 5 can be rewritten as follows to obtain a linear form of Eq. 6:

$$\frac{1}{q_t} = \frac{1}{k_2 q_e^2} + \frac{1}{q_t} t \tag{6}$$

Optimization of MB and AO7 Adsorption

An experimental design was used to optimize the factors. Central Composite Design (CCD) has resulted in 30 adsorption runs, as indicated in Table S1 (Supplementary Information). As well, we repeated each run at least 2 times. Also, the ANOVA analysis of each color is shown in Tables S2 and S3 (Supplementary Information). The main advantage of using experimental design to optimize the effective factors in an

experiment is to evaluate the interaction between the adsorption factors and their effect on the adsorbent performance. The combination of each factor with a lower and higher level of the run was done randomly. 3 ml of MB and AO7 solution was poured into a beaker and mixed with different amounts of adsorbent at different temperatures and pH. The (α-CTS-PANI-GO) film was then easily separated from the filtration solution.

Finally, the concentration of MB and AO7 was determined using a UV–visible spectrophotometer at a wavelength of 668 and 500 nm, respectively the graph of adsorption percentage in different states of the synthetic film is shown in Fig. 16. The percentage removal of MB and AO7 was determined using Eq. 7.

$$R\% = \frac{C_i - C_f}{C_i} \times 100 \tag{7}$$

Results and Discussion

Synthesis and Characterization of α-CTS-PANI-GO Film

Due to some advantages of CTS, such as low cost, renewable, non-toxic, good reactivity, and environmental compatibility, we chose CTS as the main precursor for the film preparation. As a powder material, CTS has inadequate mechanical properties and is difficult to remove from the water. In addition, the pKa values of amine groups on the backbone of CTS are 5.5–6.5 [31]. Therefore, the CTS surface charge is diminished in the physiological environment, and the CTS application is restricted to a great extent [32]. Accordingly, to optimize the physicochemical properties as well as enhance the mechanical strength of CTS, it can be modified by alpha-ketoglutaric acid to obtain functional α-CTS containing Schiff-base groups which have stronger pollutants adsorption characteristics than the non-functional CTS [33]. In the next step, we added PANI to the synthesis process of α-CTS to enhance the interaction ability of the film with organic dyes. Subsequently, to enhance the mechanical strength and dye adsorption ability of prepared CTS film GO was added to the film structure. The improvement of mechanical properties is attributed to the increase in film rigidity in the presence of GO. Finally, we investigated the effect of each component on the dye removal rate by comparing the removal ability of all CTS films prepared in this work.

X-Ray Photoelectron Spectroscopy (XPS) Analysis

XPS was used to study the stability of the synthesized film and also prove the adsorption of dye by it. As can be seen from Fig. 1a, peaks centered at 284.6 eV, 532.4 eV, and 402.3 eV are assigned to C (1s) [34], O (1_s) and N(1_s) [35]

respectively, which there are in the structure of chitosan, graphene oxide, and polyaniline. The appearance of peaks centered on 232.3 eV [36] and 152 eV [37] in the spectra of Fig. 1d and f, as well as the increase in the value of the N(1s) spectrum in Fig. 1h compared to Fig. 1c, e and g, respectively, can be attributed to the presence of MB and AO7 absorbed by the α-CTS-PANI-GO film.
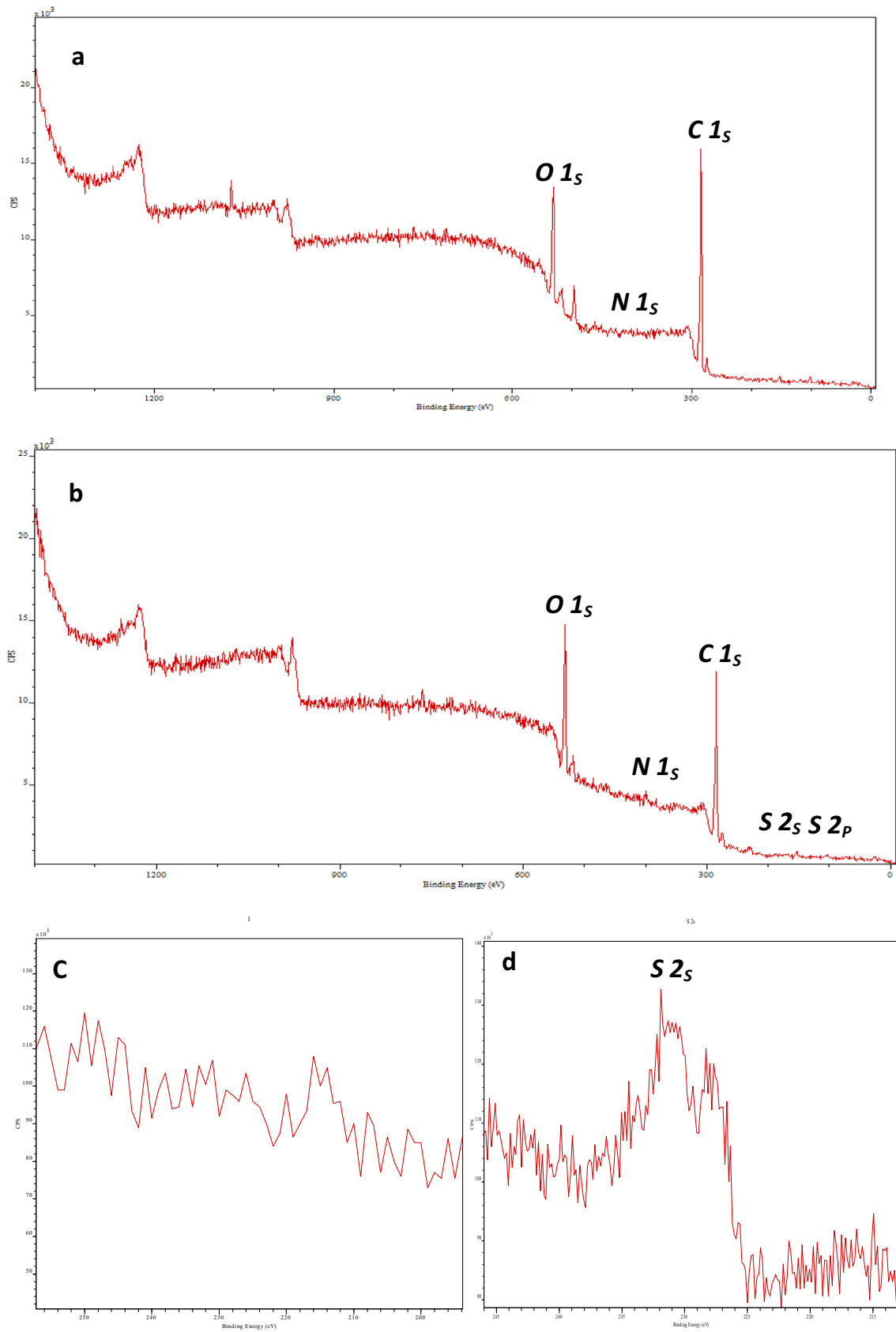
Determination of Point Zero Charge (pHpzc)

To obtain information about the nature of a charge on the surface, the zero point charge (pHpzc) of the α-CTS-PANI-GO film was determined. The film surface will have a negative charge at a pH higher than pHpzc and a positive charge at a pH lower than pHpzc [38]. The pHpzc of α-CTS-PANI-GO film was found to be at pH 4.6 (Fig. 2). Therefore, it is estimated that due to the deprotonation of functional groups in higher pH, the composite has a negative charge. Due to the positive surface charge at pH less than 4.6, the synthesized film can adsorb more anionic dye (AO7) by electrostatic interactions, which is proved by the results obtained from the experimental design. The highest adsorption percentage at pH 2 is about 97.5%. Also, according to the results obtained from the experimental design, at pH 8, due to the negative surface charge of the layer, the removal percentage of cationic dye (MB) has reached its maximum value is about 84%.According to the experimental design data, the highest percentage of adsorption was at 25°c.

Energy Dispersive X-Ray Spectroscopy (EDX)

From the EDX spectrum of the film, before the dye adsorption (Fig. 3b), the presence of carbon, oxygen, and nitrogen elements in the spectrum before adsorption indicates the presence of four compounds, α-ketoglutaric acid, chitosan, polyaniline, and graphene oxide in the structure of the synthetic film. After the dye adsorption, we found that both dye compounds were absorbed by the film (Fig. 3a). The increase in weight of carbon and sulfur elements on the film after adsorption indicates the adsorption of dye compounds. In addition, EDX elemental mapping (Fig. 4a) shows the uniform distribution of carbon, sulfur, and nitrogen on the surface. The data obtained from the analysis concluded that anionic and cationic dyes were absorbed simultaneously.

X-Ray Diffraction Analysis (XRD)

The crystallinity of the polymer is a very important factor that determines its mechanical properties as well as its stability and biological response. In Fig. 5a, the sharp peak at 15.48° in the (chitosan/graphene oxide) pattern is the result of the anhydrous crystalline structure in the CTS matrix. (CTS-PANI-GO) composite showed a significant
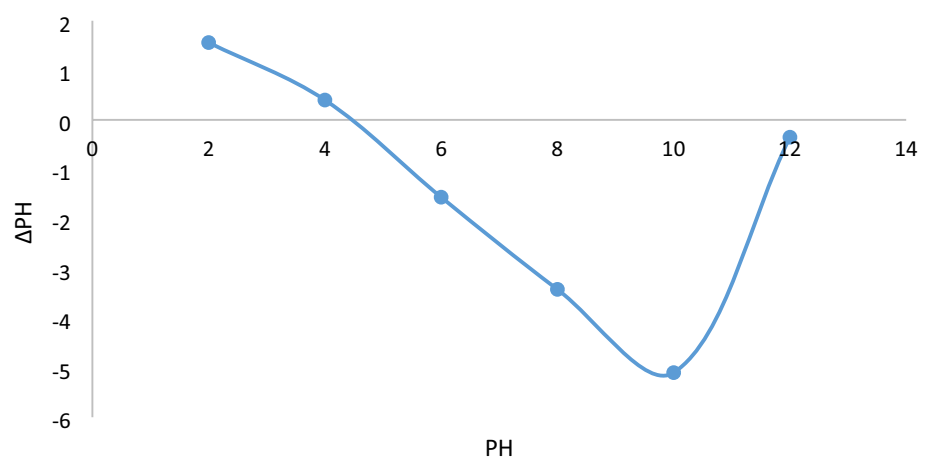
**Fig. 1** XPS spectrum **a**, **c**, **e**, **g** before adsorption, **b**, **d**, **f**, **h** after adsorption
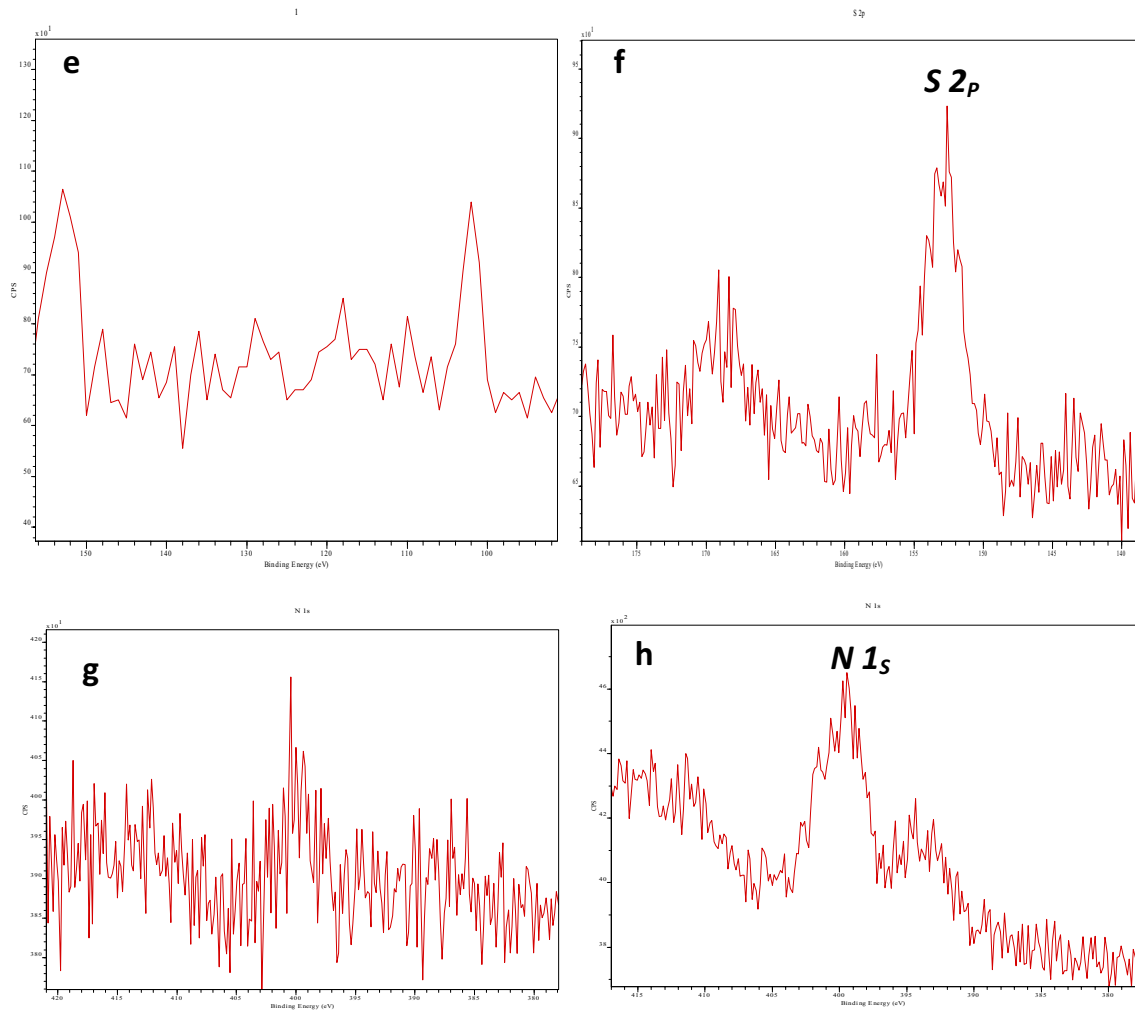
Fig. 1 (continued)

Fig. 2 Determination of point zero charge (pHpzc) α-CTS-PANI-GO film

increase in the peaks assigned to CS crystalline forms. Two peaks were found at 18 and 20 degrees. This phenomenon can be attributed to the synergistic effect of GO

and PANI as crosslinkers. As shown in Fig. 5b, all the samples of α-ketoglutaric acid-based composites showed

Element	Wt%
C	47.33
O	50.12
N	2.47
S	0.08

Element	Wt%
C	57.66
O	37.91
N	4.41
S	0.02
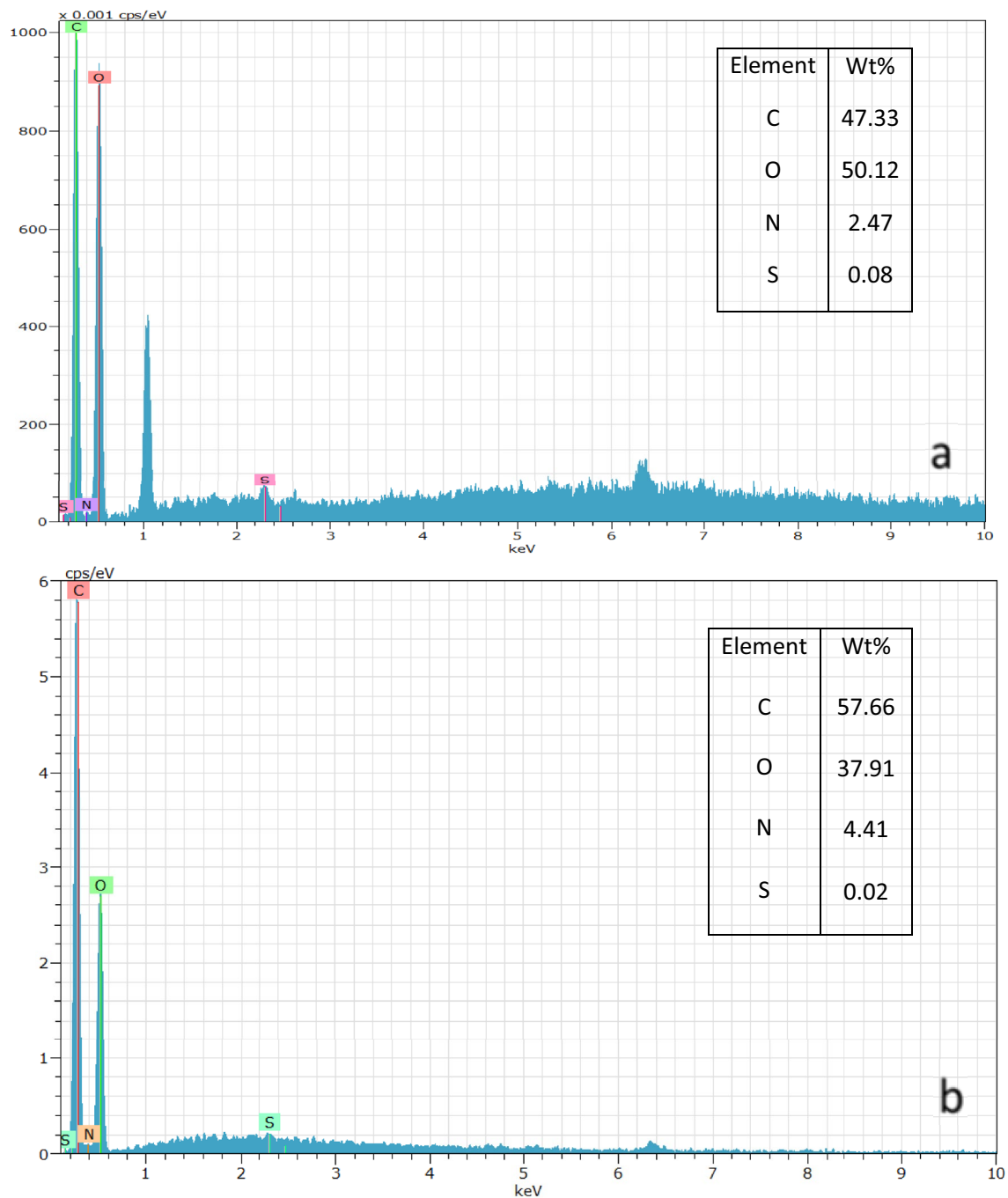
Fig. 3 EDX spectrum **a** after adsorption, **b** before adsorption

an amorphous or almost completely amorphous characteristic, the increase in the intensity of the spectrum as well as its width after the adsorption process indicated the presence of new carbon compounds. The increase in peak strength related to carbon and nitrogen atoms after adsorption can be related to the dyes absorbed by the synthesized film.

Regeneration of α-CTS-PANI-GO Film

To investigate the possibility of reusing α-CTS-PANI-GO film, it was regenerated by washing in HCl at a concentration of 0.01 M. After the treatment, α-CTS-PANI-GO film was used to absorb pollutants in fresh wastewater under the same optimal conditions. Acid washing allows the use of regenerated α-CTS-PANI-GO film. This is due to the
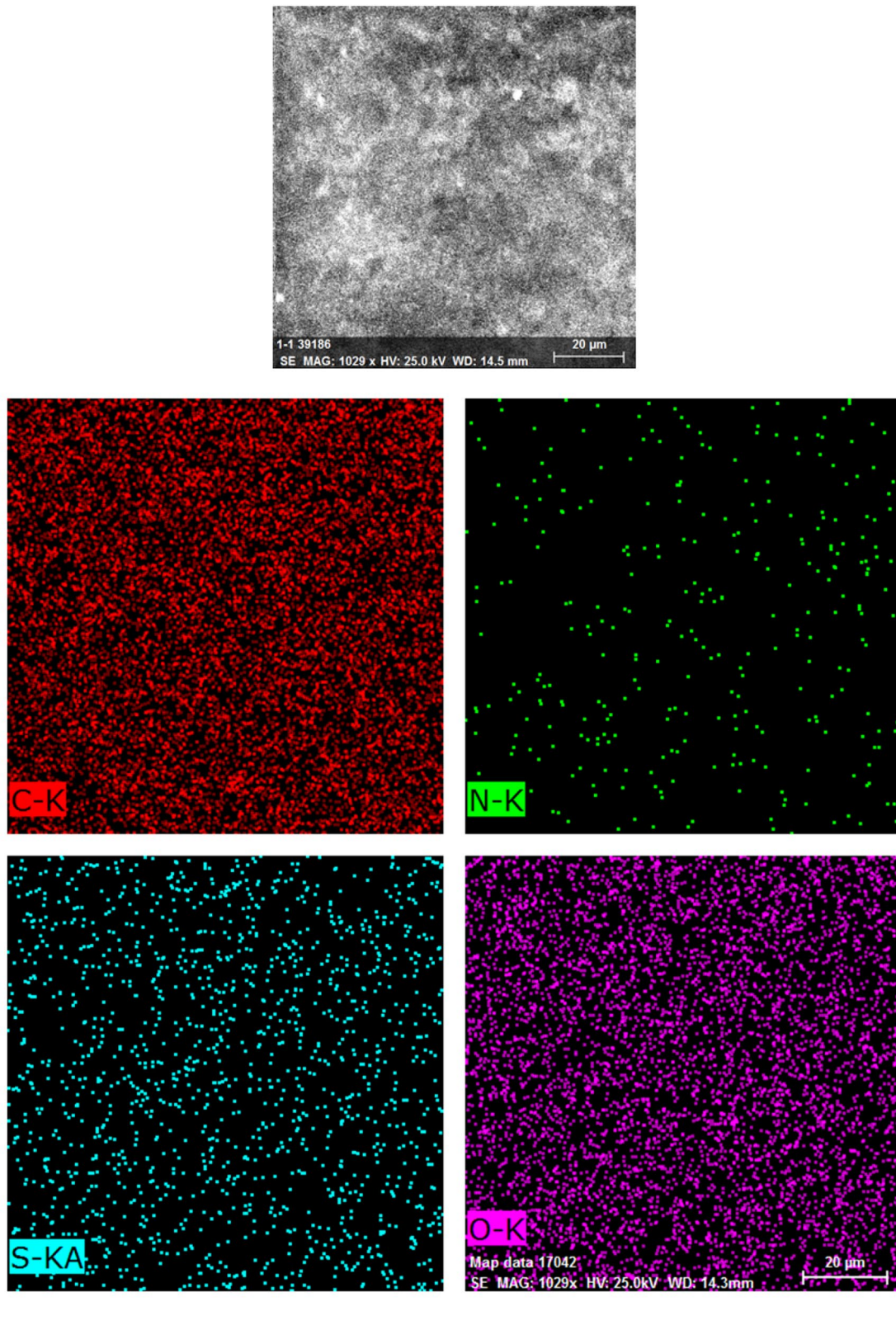
Fig. 4 EDX elemental mapping **a** after adsorption, **b** before adsorption
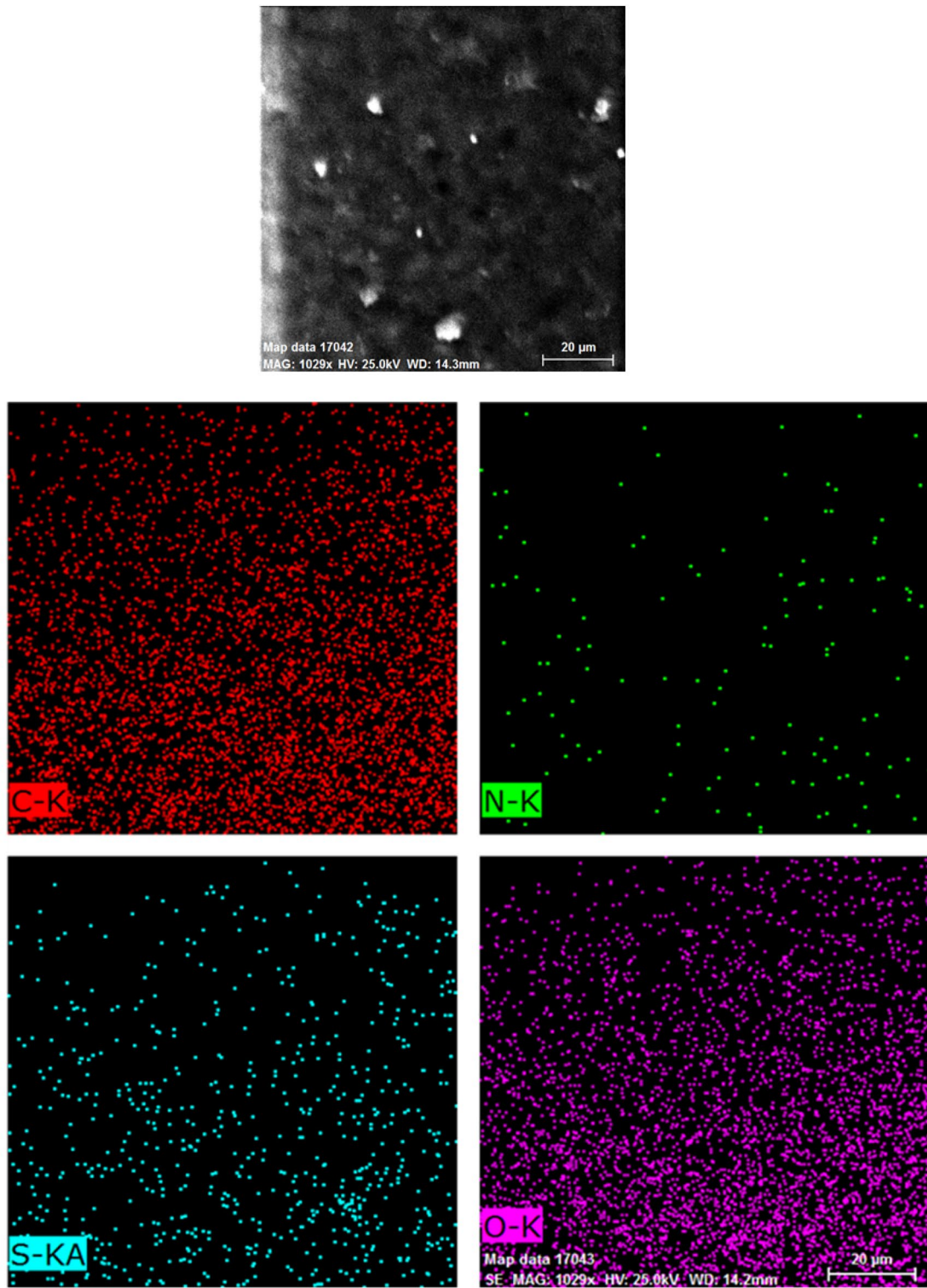
C-K, N-K, S-KA, O-K,
Date:2/19/2016 3:50:36 PM
Image size:400 x 400
Mag:1029.49061662198x
HV:25.0kV

(b)

Fig. 4 (continued)

**Fig. 5** **a** Before adsorption, **b** after adsorption
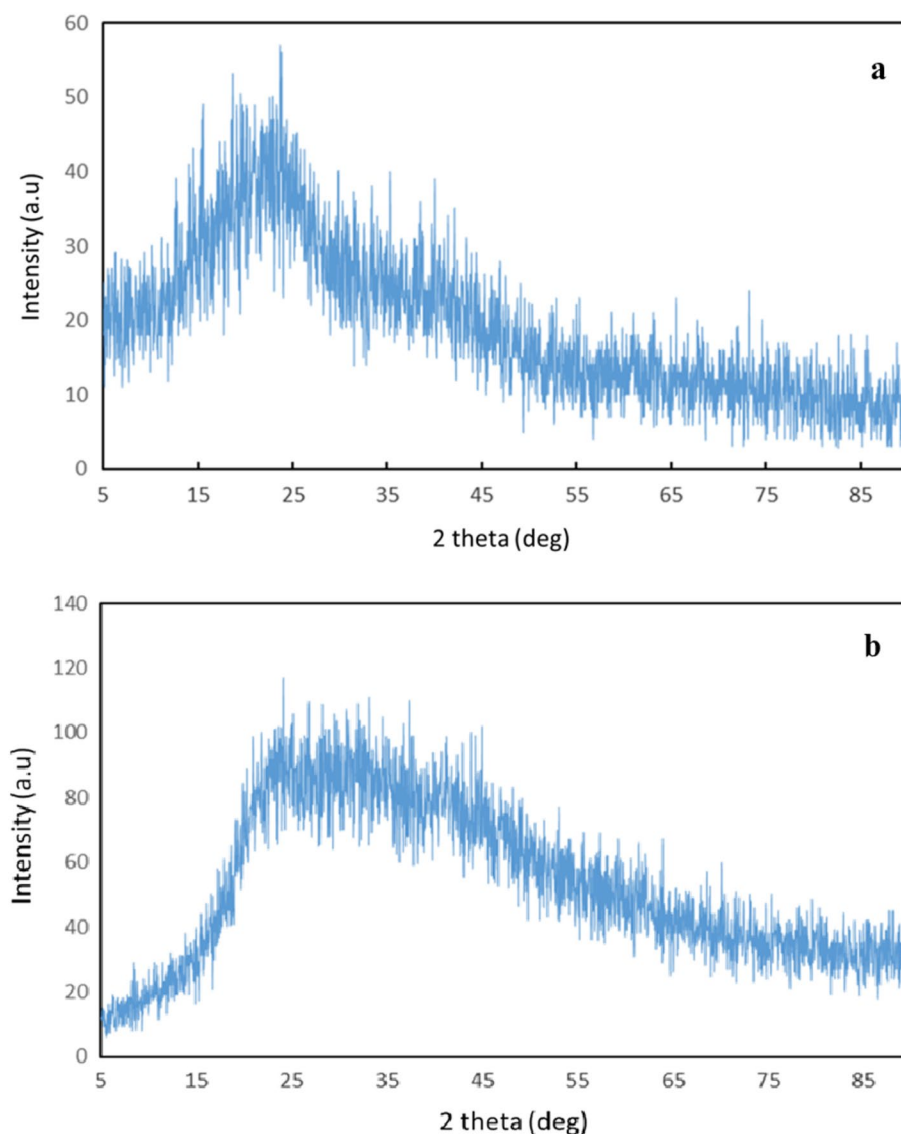
presence of acid concentration It leads to repulsive electrostatic interactions [39] between the α-CTS-PANI-GO film and pollutants, which leads to the repulsion of more dyes from the α-CTS-PANI-GO film surface. Also, the adsorption capacities of the regenerated film decreased with the increase in the number of regenerations (Fig. 6), because the regeneration of α-CTS-PANI-GO film with any of the chemicals cannot completely remove all the adsorbed pollutants. When α-CTS-PANI-GO film was used repeatedly, the accumulation of dyes on the surface of α-CTS-PANI-GO film increased, leading to a decrease in the number of available adsorption sites on α-CTS-PANI-GO film.

Fourier Transform Infrared Spectroscopy (FTIR)

According to (Fig. 7a), various oxygen configurations in the structure include the vibration modes of epoxide (C–O–C)

(1230–1320 cm^{-1}), sp^2-hybridized C=C (1500–1600 cm^{-1}, in-plane vibrations), carboxyl (COOH) (1650–1750 cm^{-1} including C–OH vibrations at 3530 cm^{-1}), and hydroxyl (namely phenol, C–OH) (3050–3800 and 1070 cm^{-1}) with all C–OH vibrations from COOH and H$_2$O (a) [40]. In the FTIR spectrum of PANI (Fig. 7b), a broad band at 3446 cm^{-1} was assigned to the free N–H stretching vibration. The ring stretching of quinoid and benzenoid form is observed at 1563 and 1476 cm^{-1}, respectively. The C–N stretching band of an aromatic amine appears at 1296 cm^{-1}. Polyaniline shows a strong band at 1110 cm^{-1}, which has been explained as electronic-like adsorption of N=Q=N (Q=quinoid ring) [41]. For the CTS, the characteristic adsorption bands of amide structures appeared at 1624 cm^{-1} (amide I, C=O stretching vibration), 1544 cm^{-1} (amide II, N–H bending vibration), and 1461 cm^{-1} (amide III, C-N stretching vibration) (Fig. 7c) [42]. The peak located at 3100–3600 cm^{-1}

Fig. 6 Adsorption capacity of **a** MB, **b** AO7 by α-CTS-PANI-GO film successively regenerated with (HCl 0.01 M)
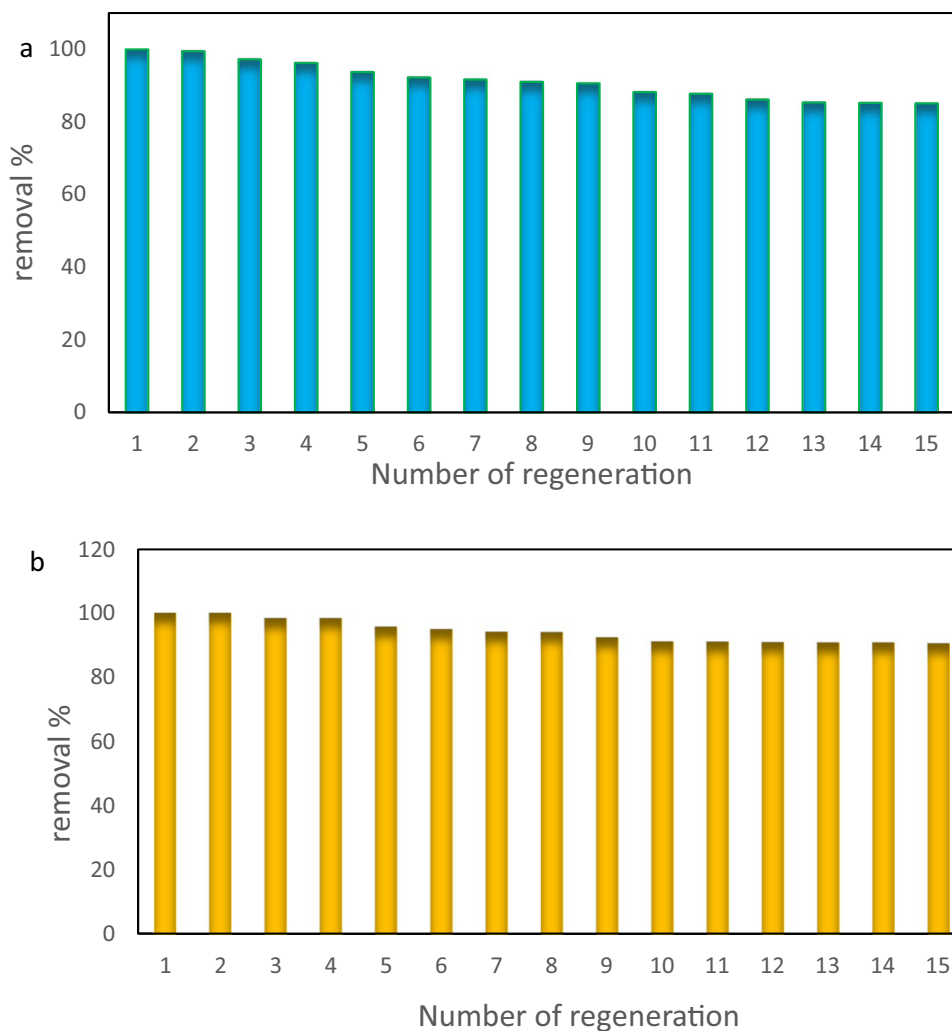
is attributed to the stretching vibration of –OH and –NH$_2$. For FTIR spectra of α-CTS film (Fig. 7d), it can be clearly seen that the chemical modification significantly altered the FTIR spectrum of CTS; the new adsorption band located at 1718 cm^{-1} corresponds to the stretching vibration of C–O. In addition, the new adsorption bands located at 1560 and 1399 cm^{-1} correspond to the antisymmetric and symmetric stretching vibration of C=O. which is a multi-electron conjugated system in which two C–O oscillations are coupled [20]. The α-CTS-PANI hybrid shows the significant characteristic bands of both α-CTS and PANI with some redshifts to the lower wave numbers, which can explain the interaction between CTS and PANI chains. The characteristic band at 3448 cm^{-1} is assigned to the stretching vibration of O–H and N–H groups of CTS and PANI. The bands at 2924 cm^{-1} prove the presence of –CH groups of PANI, and the band at 1629 cm^{-1} is assigned to C=C of the quinoid structure of PANI. The band observed at 1120 cm^{-1} is assigned to the secondary hydroxyl group (characteristic peak of –CH–OH in cyclic alcohol, C–O stretch) and the primary hydroxyl

group (characteristic peak of –CH$_2$–OH in primary alcohol, C–O stretch) of CTS, respectively (Fig. 7e) [43]

According to Fig. 8, the FT-IR spectrum of (α-CTS-PANI-GO) film revealed characteristic peaks at around 3420 and 1736 cm^{-1} corresponding to O–H and C–O stretching frequencies of the –COOH group, respectively. The peaks corresponding to aromatic C–C bending, phenolic C–O stretching, and epoxy C–O–C stretching were identified at 1628, 1226, and 1052 cm^{-1}, respectively [44]. In comparison with the results obtained for α-CTS-PANI-GO film, after adsorption of dyes, the intensity of all specific peaks of α-CTS-PANI-GO film, which are related to the –O–H and –C–O groups, is decreased. These results indicate the adsorption of MB and AO7 onto the film.

Scanning Electron Microscope (SEM) and Raman Analysis Surface morphology in each step of film synthesis has been studied by FE-SEM image. Figure 9a shows the FE-SEM image of a bare chitosan film. As can be seen, the chitosan layer has a smooth and uniform surface structure.
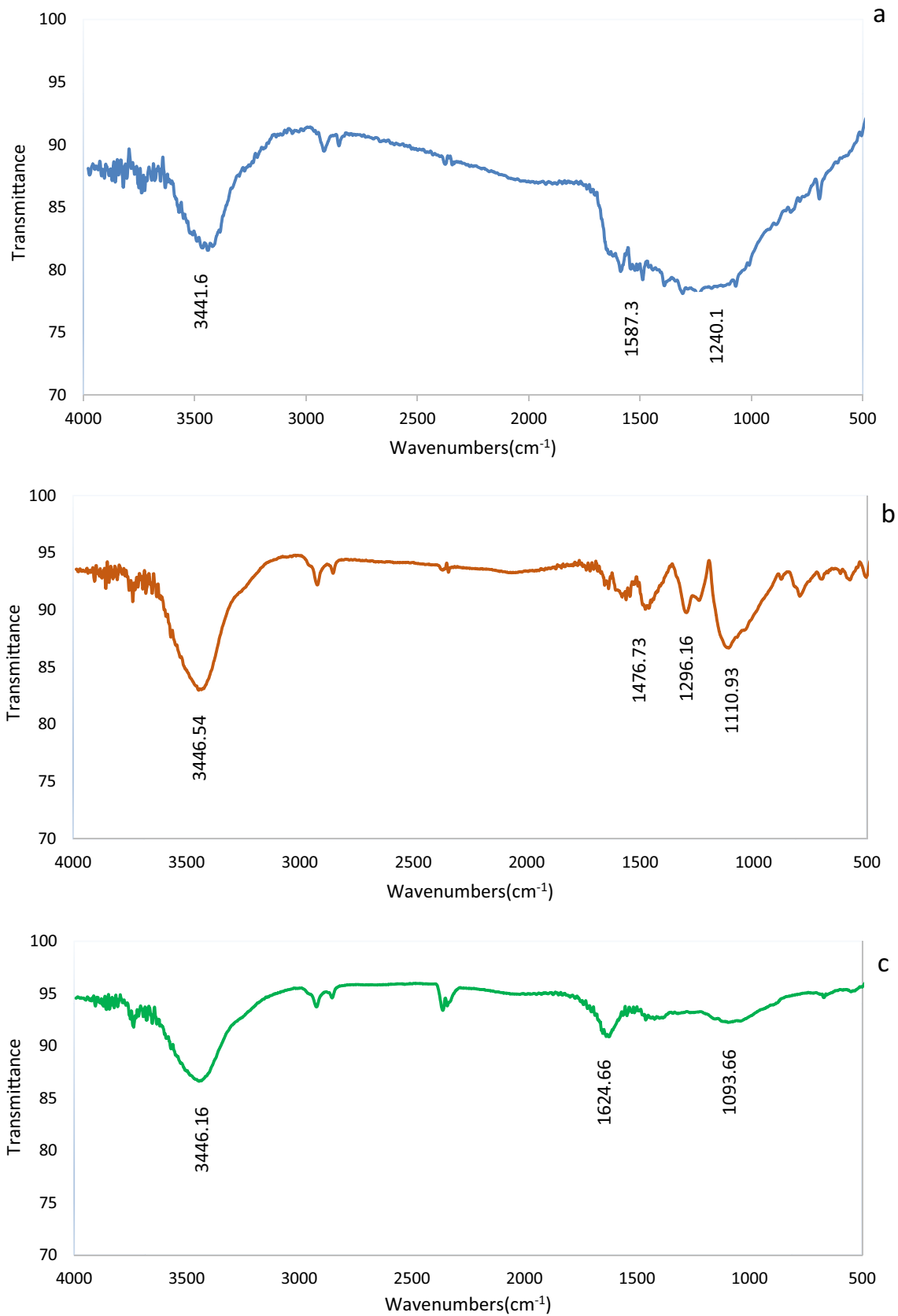
Fig. 7 FTIR spectrum of GO (**a**), PANI (**b**), chitosan (**c**), chitosan-α-ketoglutaric acid (**d**), chitosan-α-ketoglutaric acid-PANI (**e**)
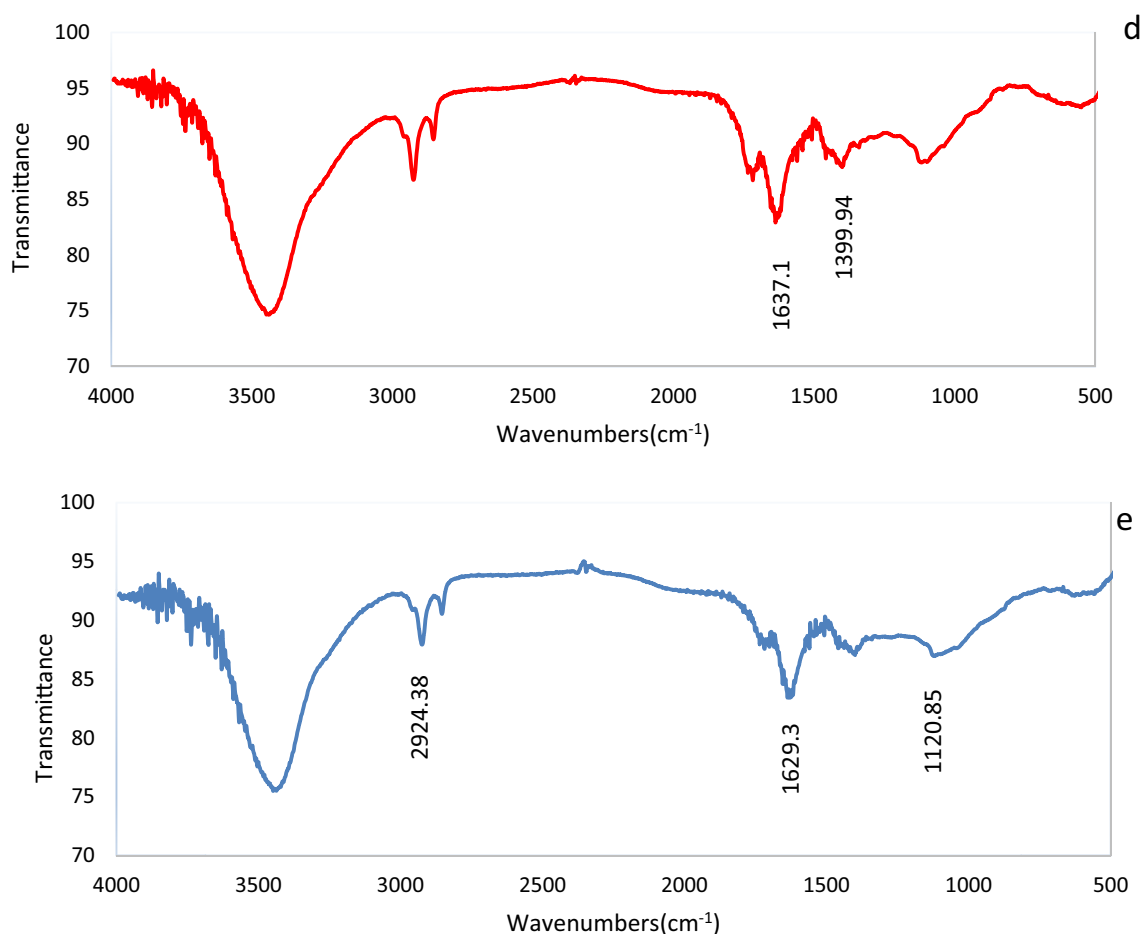
Fig. 7 (continued)

Figure 9b shows the FE-SEM Image of the film, where GO and PANI are placed on the surface of CTS. Raman investigation is a useful method to study and investigate the disorder in the crystal structure and is used to identify the compounds of graphene and its derivatives. Figure 10 shows the Raman of a hydrogel sample containing CS chitosan, GO graphene oxide, and PANI polyaniline. The presence of two adsorption bands, D and G, in the Raman format is characteristic of the formation of graphene oxide, and structural irregularities are determined from the intensity ratio of these two bands, I_D/I_G, and the ratio of the intensity of these two peaks, I_D/I_G, is approximately 0.96 [45]. According to the Fig. 11, the presence of adsorption bands D at 1345 cm^{-1} and G at 1603 cm^{-1} is a confirmation of the irregularities of the graphene oxide network and the interaction with CS and PANI. The G band is related to the E_{2g} photons of sp^2 carbon atoms, the carbon–carbon double bond, and the D band is related to the sp^3 carbon atom vibrations in the graphene oxide structure [46]. The double and wide 2D band of another characteristic of graphene oxide (Fig. 11) at 2835 and 2932 cm^{-1} indicates the formation of multilayered

graphene oxide along the c axis in the studied composition [44]. For the PANI compound, the C–H bending vibration in the benzenoid ring is 1169 cm^{-1}, the C–N^+ stretching vibration is 1329 cm^{-1}, the C=N stretching vibration is 1509 cm^{-1}, and the C=C stretching vibrations in the quinoid are in 1597 cm^{-1} appear, which show the presence of PANI structure on graphene oxide [47, 48]. In confirmation of the presence of CS species in this structure, the stretching region of C_C 1290–1350cm^{-1}, amide-III 1445 cm^{-1}, amide-II 1580 cm^{-1}, and amide-I 1639 cm^{-1} appears [49], which overlaps with other peaks to some extent, but the presence of adsorption bands at 935 cm^{-1} (CN), 1587 cm^{-1} (NH) and 1639 cm^{-1} (C=O) indicates the presence of CS in this compound [50]. The desired composition was studied and investigated for absorbing two pollutants, AO7 and MB. Figure 12 shows the comparison of the Raman spectrum of the studied sample before and after adsorption. According to the shape of the spectrum after adsorption, it shows changes in the intensity ratio of I_D/I_G, which decreased from 0.96 to 0.84 [51]. This value shows the change in the electron states of graphene oxide in the adsorption process. The increase
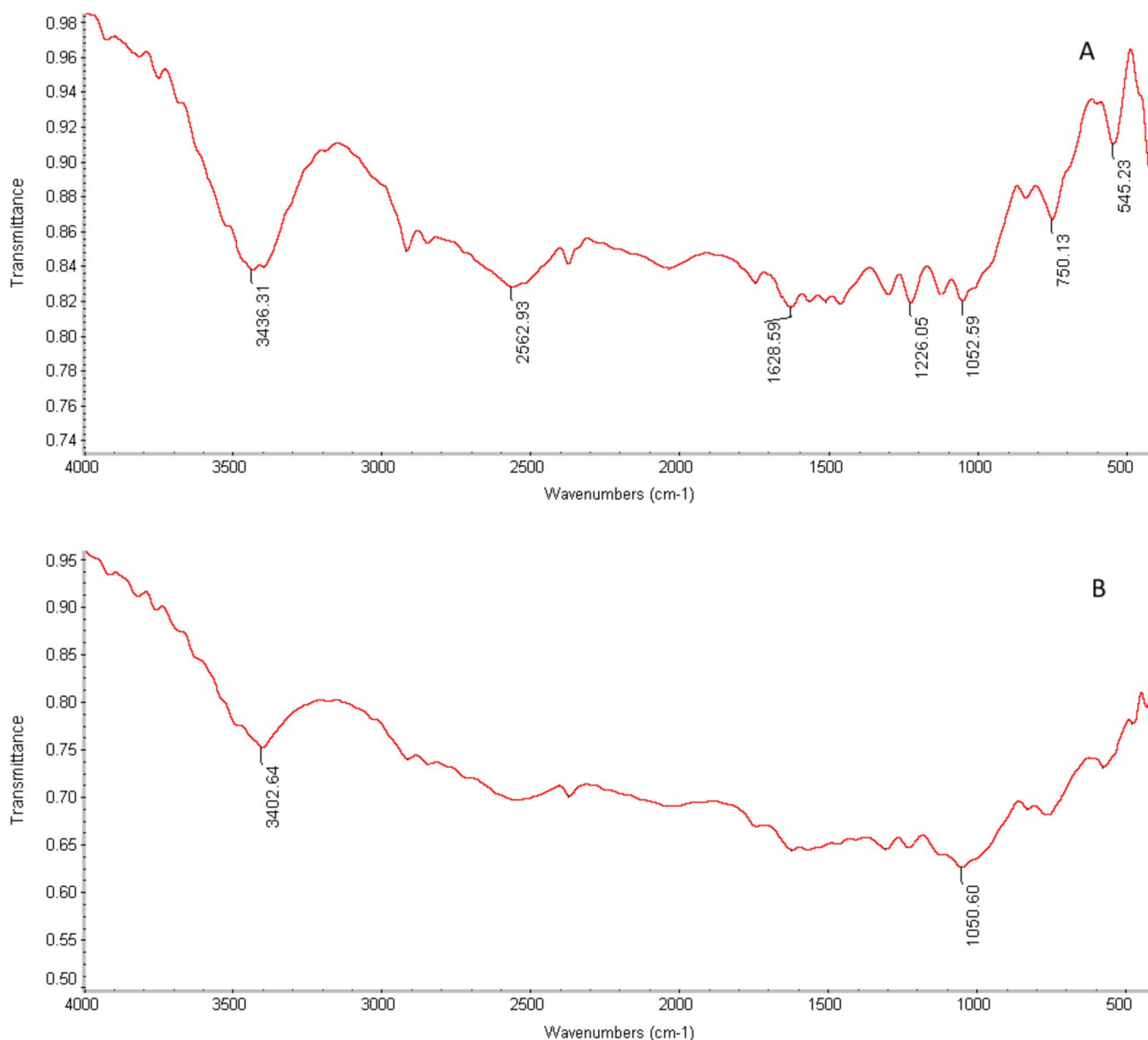
Fig. 8 FTIR spectrum of (α-CTS-PANI-GO) film, before adsorption (**A**), after adsorption (**B**)

in the intensity of the G band, which represents carbon–carbon double bonds, can be attributed to the existence of π–π stacking interactions between the benzene rings in graphene oxide and MB and AO7 [52]. Also, all three compounds of GO, CTS, and PANI have active groups OH, O^{2-}, NH, and N^+, which are active sites for absorbing various anionic and cationic pollutants. As a result, the presence of these 3 types in a composition can increase its adsorption capacity. The increase in the intensity of the peaks in the region between 1450 and 1550 cm^{-1}, which indicates the stretching vibrations of C=N groups in PANI, can be proof of the presence of interactions between pollutant species with this site of PANI. Also, the increase in intensity of the peak at

1160–1230 cm^{-1} (C–N^+ stretching vibration) can be attributed to the interaction with MB cationic dye [53, 54]. The CTS is also active in the adsorption process due to having amine and hydroxyl groups, and the shift of its characteristic peak to 1639 cm^{-1} can also be a reason for creating a new interaction with polluting species [55, 56].

Central Composite Design (CCD) Model and Data Analysis

An experimental design was used to optimize the factors. Central Composite Design (CCD) has resulted in 30 adsorption runs, as indicated in Table S1 (supplementary
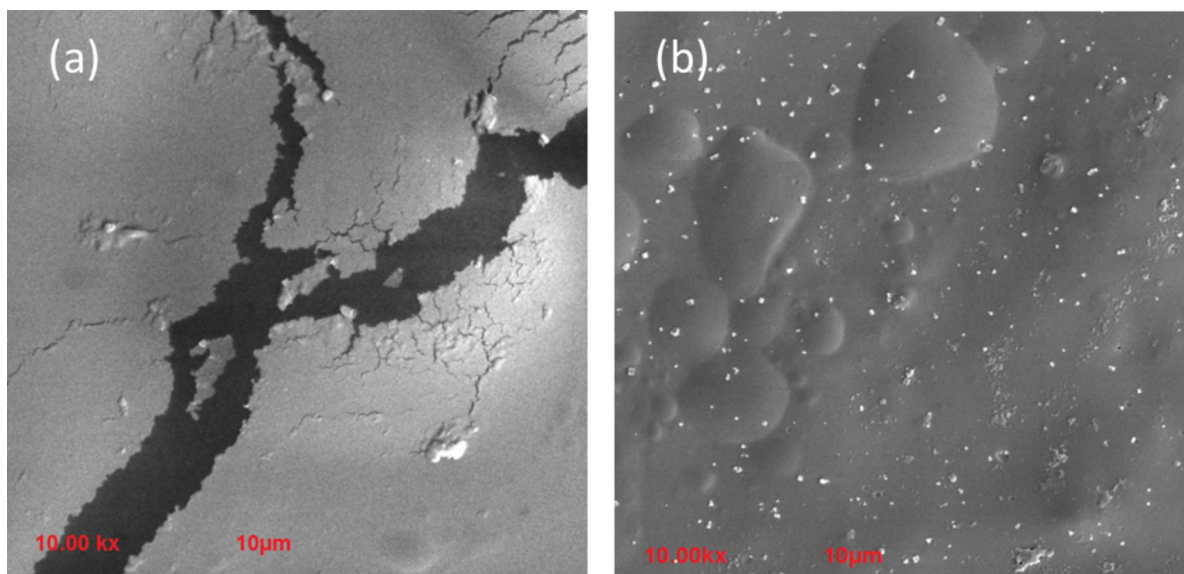
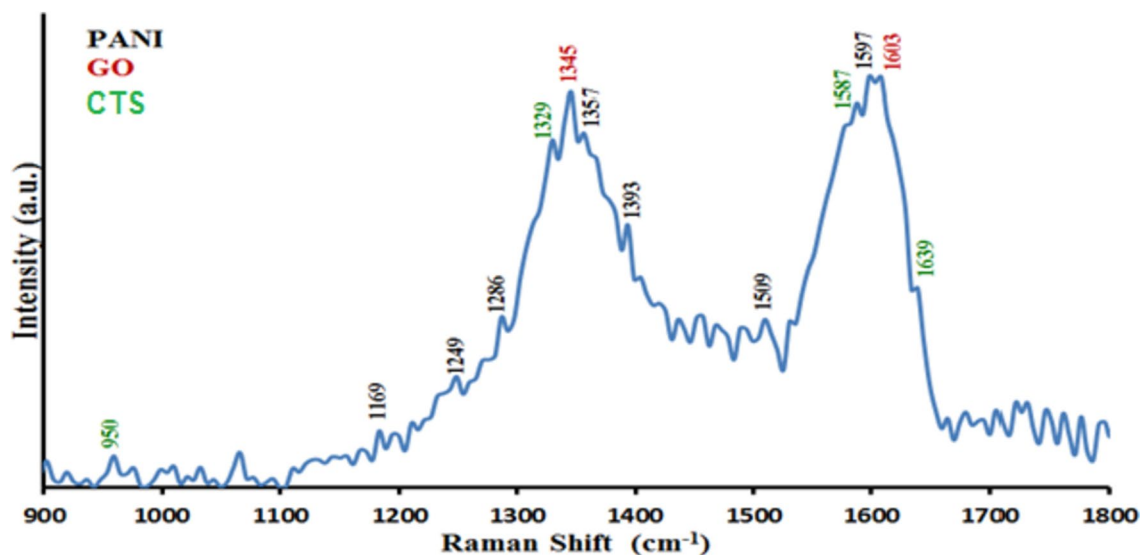**Fig. 9** FE-SEM images of chitosan (**a**) and α-CTS-PANI-GO film (**b**)

Fig. 10 Raman spectrum of (α-CTS-PANI-GO) film sample before adsorption of polluting dyes

information). Also, the ANOVA analysis of each color is shown in Tables S2 and S3 (supplementary information). Independent parameters described in terms of the coded parameters, Adsorbent (g) D, Temperature (°C) C, Time (min) B, pH A, by the second-order polynomial equation as given in Eqs. 8 and 9 for AO7 and MB, respectively

$$
\begin{aligned}
Y(AO7) = {} & 86.0815 + -9.04727 * A + 4.41893 * B \\
& + 5.56758 * C + 4.83872 * D + 3.95924 * AB \\
& + 1.32284 * AC + -1.18682 * BC \\
& + -0.457775 * BD + -0.976375 * CD \\
& + -1.54549 * A^2 + 1.55238 * ABC \\
& + -1.3824 * ACD + -1.49009 * BCD \\
& + -1.32344 * A^2B + -4.04649 * A^2C \\
& + 8.61482 * AB^2
\end{aligned}
$$

$$(8)$$
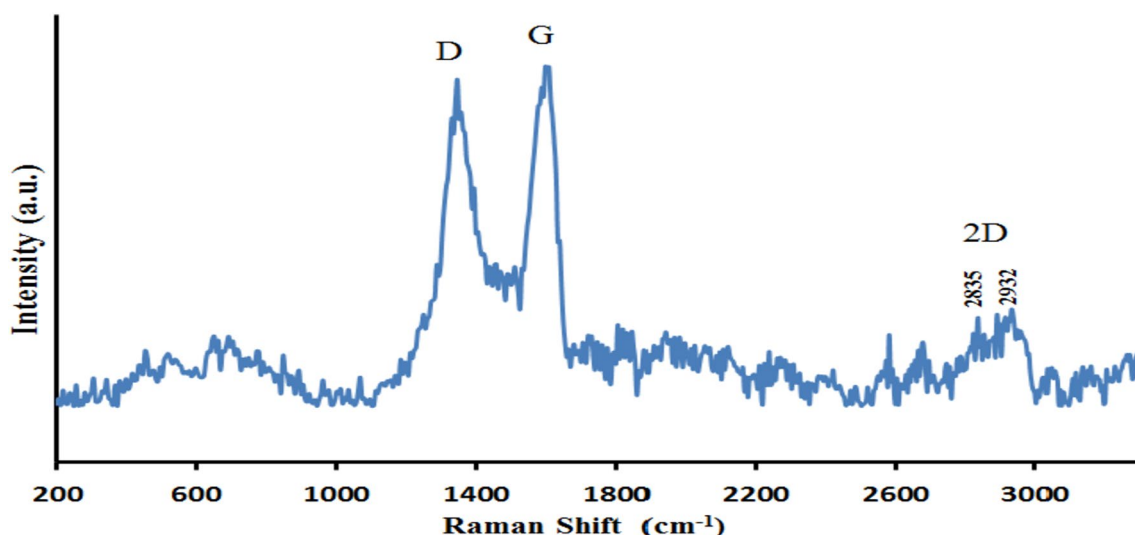
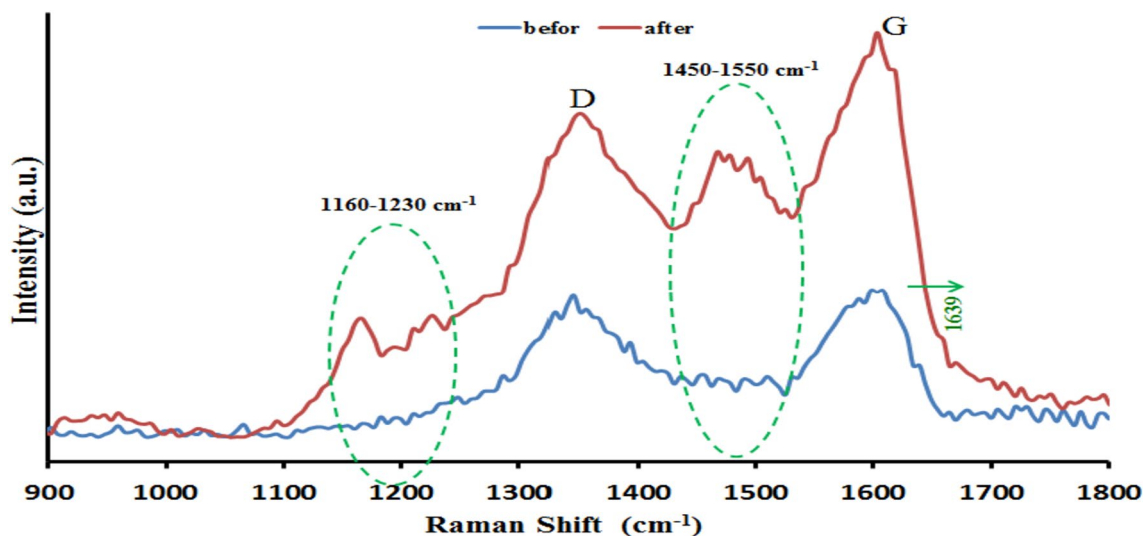**Fig. 11** Raman spectrum of (α-CTS-PANI-GO) film sample before adsorption of polluting dyes

Fig. 12 Comparison of Raman spectrum of (α-CTS-PANI-GO) film sample before and after adsorption of polluting dyes

$$
\begin{aligned}
Y(MB) =\ & 69.8429 + 3.8111 * A + 0.60785 * B \\
& + 2.58619 * C + 6.43953 * D + 2.56853 * AB \\
& + -1.02627 * AC + 1.05576 * AD \\
& + -0.5012 * BD + -0.2234 * CD \\
& + -1.07156 * A^2 + 1.10524 * B^2 \\
& + 0.28008 * C^2 + -0.493013 * ABC \\
& + -0.386175 * ABD + 3.8221 * A^2B \\
& + -2.52296 * A^2D + -2.60479 * AB^2
\end{aligned}
\tag{9}
$$

The correlation coefficient (R^2) was used for the determination of the relationship between experimental and predicted data, and the values of 0.9652 and 0.9532 were provided by the model for MB and AO7, respectively. Furthermore, the analysis of variance (ANOVA) was used to determine the adequacy of the model [Tables S2 and S3 (supplementary Information)]. The complete diversity of the results obtained by ANOVA is divided into two variations: One is related to the model and the other is related to experimental errors and thus determines whether the change is significant from the model or not. It is calculated by the factor F-value which is expressed as the square-to-residual error ratio of the mean model. The F-value obtained in the present study was 19.55 and 22.50, which suggested the fitness of the response surface model for
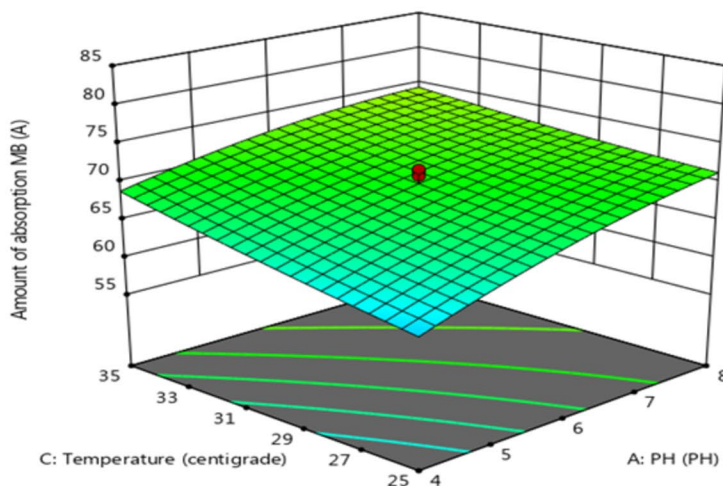
Fig. 13 Combined effect of factors A–C on adsorption percentage MB (**a**), Combined effect of factors B–C on adsorption percentage AO7 (**b**)

MB and AO7, respectively. The values of Prob > F less than 0.0500 showed that the terms are significant [57]. It is found that A, C, D, AB, and A^2 were the significant model terms, whereas BD, CD, A^2, and B^2 were the insignificant t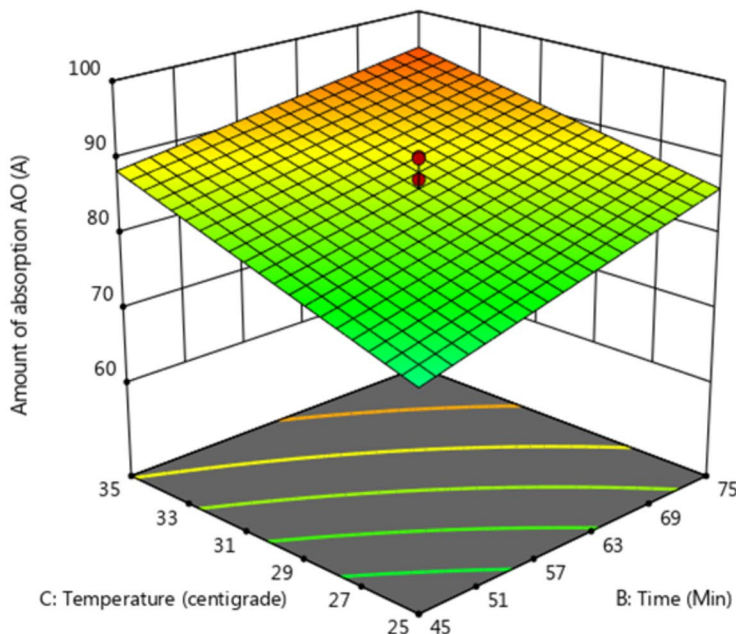erms for adsorption of MB and A, B, C, D, AB, A^2, ABC, ACD, BCD and AB^2 were the significant model terms, whereas AC, BC, BD and A^2B were the insignificant

terms for adsorption of AO7. Figure 13a represents the 3D surface plot of the adsorption percentage MB at a constant initial MB concentration as a function of temperature (C) and pH of the solution (A). It can be seen that with the increase in pH and temperature, the adsorption percentage of MB reaches its maximum. Figure 13b represents the 3D surface plot of the adsorption percentage AO7 at

Table 1 Calculated values of the various kinetic models' constants and their correlation coefficients (R2) for adsorption of MB and AO7

Kinetic model	q_e	R^2	K	RMSE
Pseudo-first-order	0.06	0.99	0.0166	0.01
Pseudo-second-order	0.10	0.95	0.2077	0.00

Table 2 Calculated values of the various isotherm model constants and their correlation coefficients (R2) for adsorption of MB and AO7

Model	Parameter
Langmuir AO7	$q_{max} = 285.71$ $k_l = 0.099$ $R^2 = 0.9873$
MB	$q_{max} = 232.56$ $k_l = 0.12$ $R^2 = 0.9874$
Freundlich AO7	$n = 0.29$ $K_f = 1.45$ $R^2 = 0.9732$
MB	$n = 0.3$ $K_f = 1.04$ $R^2 = 0.9558$

a constant initial AO7 concentration as a function of temperature (C) and time (B). It can be seen that with the increase in temperature and time, the adsorption percentage of AO7 reaches its maximum.

Kinetic Study

The obtained adsorption data were used to study the dynamic of the adsorption process in terms of the order of rate constant. Firstly, kinetic data was studied with the quasi-order kinetic model. By plotting log (q_e/q_t) in terms of t values of equilibrium adsorption capacity (qe) values, the velocity constant (k_1), the root mean square of the errors (RMSE), and the correlation coefficient (R^2) were calculated, which

are presented in Table 1. RMSE estimated the error of the residues obtained from regression lines made to obtain kinetic parameters. The calculated equilibrium adsorption capacities agree with experimental values. The calculated (q_e) values have a very good correlation with the laboratory data, which shows that the adsorption of MB and AO7 follows the quasi-order kinetic model. The correlation coefficient for the quasi-order kinetic model is higher than 0.99 in this case.

The quasi-second-order kinetic model was used to study the kinetic data [45, 58]. If the plot of t/q_t versus t shows a linear relationship, we can say that the second-order kinetics is quasi-applicable. The equilibrium adsorption capacity (q_e), the correlation coefficients (R^2), the second-order rate constant (k_2), and the root mean square of the errors (RMSE) obtained from the regression line are shown in Table 2. The calculated equilibrium adsorption capacities do not agree with experimental values. This indicated that the adsorption of MB and AO7 onto (α-CTS-PANI-GO) film is not a quasi-second-order kinetic reaction.

Adsorption Isotherms

MB and AO7 adsorption was studied at different initial MB and AO7 concentrations of 0.5, 1, 1.5, 2, 2.5 and 3 mg/L at the fixed adsorbent dose of 0.004 g/50 ml, contact time 60 min, and pH 6. Langmuir and Freundlich's isotherms were used to study the homogeneity and heterogeneity of the adsorbent surface. The linearized Eq. (10) of the Langmuir

Fig. 14 Langmuir isotherm plot of AO7 (**a**), MB (**b**)
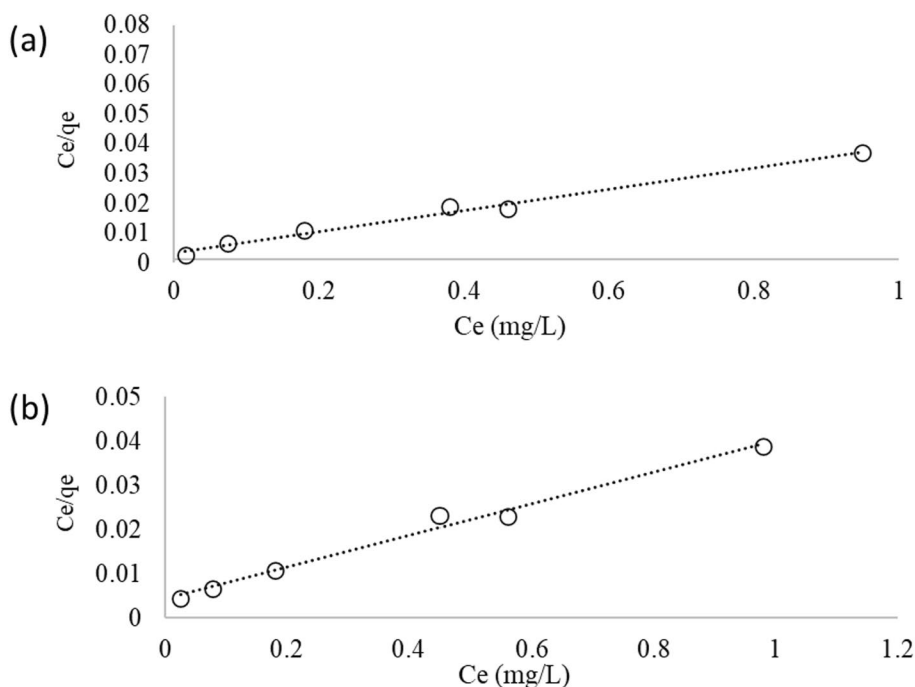
isotherm was used and the design results are shown in Fig. 14.

$$\frac{C_e}{q_e} = \frac{1}{q_{max}}C_e + \frac{1}{K_{qmax}} \qquad (10)$$

From the plot of C_e vs. C_e/q_e, the value of q_{max} was calculated from the slope ($1/q_{max}$) of the linearized equation of the Langmuir for each of MB and AO7. Thus, the q_{max} value of 232.56 and 285.71 was found for MB and AO7, respectively. Similarly, the Langmuir constant (K_L) was calculated from the intercept of the graph ($1/(q_{max} K_L)$), and its result of 0.12 for MB and 0.099 for AO7 was recorded. The calculated R^2 value obtained was 0.98 and 0.98 for MB and AO7, respectively. Based on this analysis, the experimental data AO7 was also best fitted with the Freundlich isothermal model. In general, the adsorption of AO7 on (α-CTS-PANI-GO) film was favorable, and the value of R^2 from the diagram was close to 1, which indicates that the adsorption process is a homogeneous and single layer, and the Langmuir model describes the best adsorption mechanism. All the isotherm data are shown in Table 2.

The Mechanism of Adsorption

The adsorption mechanism of MB and AO7 dye by chitosan can be elucidated through two primary modes of interaction, as depicted in Fig. 15: (1) Electrostatic interactions: MB contains a positively charged group (S+), which can interact with the negatively charged groups on chitosan (–COCH3), leading to electrostatic attractions between the two molecules. (2) Hydrogen bonding: MB dye contains nitrogen atoms in its structure, which can act as hydrogen-bond acceptors [59]. From the chemical structure of MB, we could speculate that the adsorption of MB also involves π–π stacking interactions. In addition, hydrogen bonding between the hydroxyl of GO and the nitrogen of MB The probable adsorption mechanism of MB by GO is schematically represented in Fig. 15 [60]. In many cases, the adsorption of dyes such as AO7 on CTS is executed by the involvement of electrostatic interactions, electrostatic attraction, and hydrogen bonding.

Synergistic Effect

To investigate the synergistic effect of various components of the film, seven types of fabricated film with different compositions were added to the dye solution at the same conditions. By measuring the adsorption percentage for the AO7 at the wavelength of 500 and MB at 668 nm before and after the adsorption, it was determined that the participation of GO, PANI, and α-ketoglutaric acid in CTS film preparation shows a significant synergistic effect in the dye removing (Fig. 16). According to Table 3, the adsorption capacity of the film prepared in this work has increased optimally compared to other similar works. According to the research work by Zhou et al. for alizarin red removal, mechanistically, π–π stacking interaction and electrostatic interaction

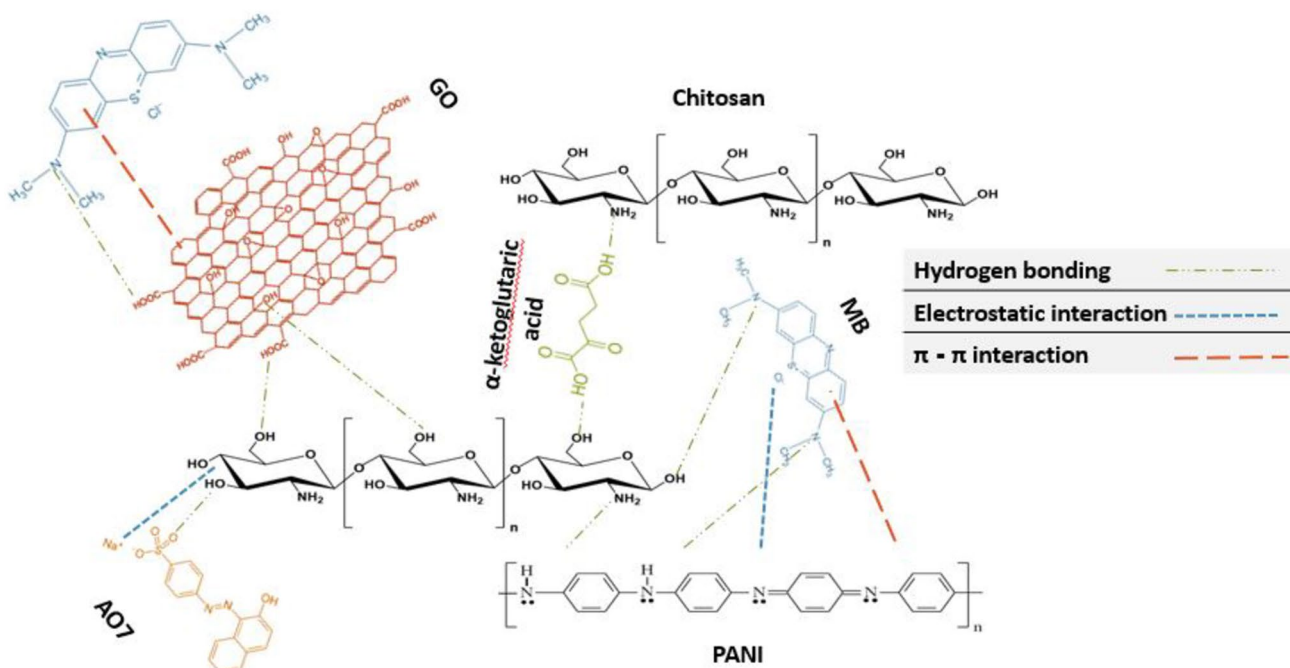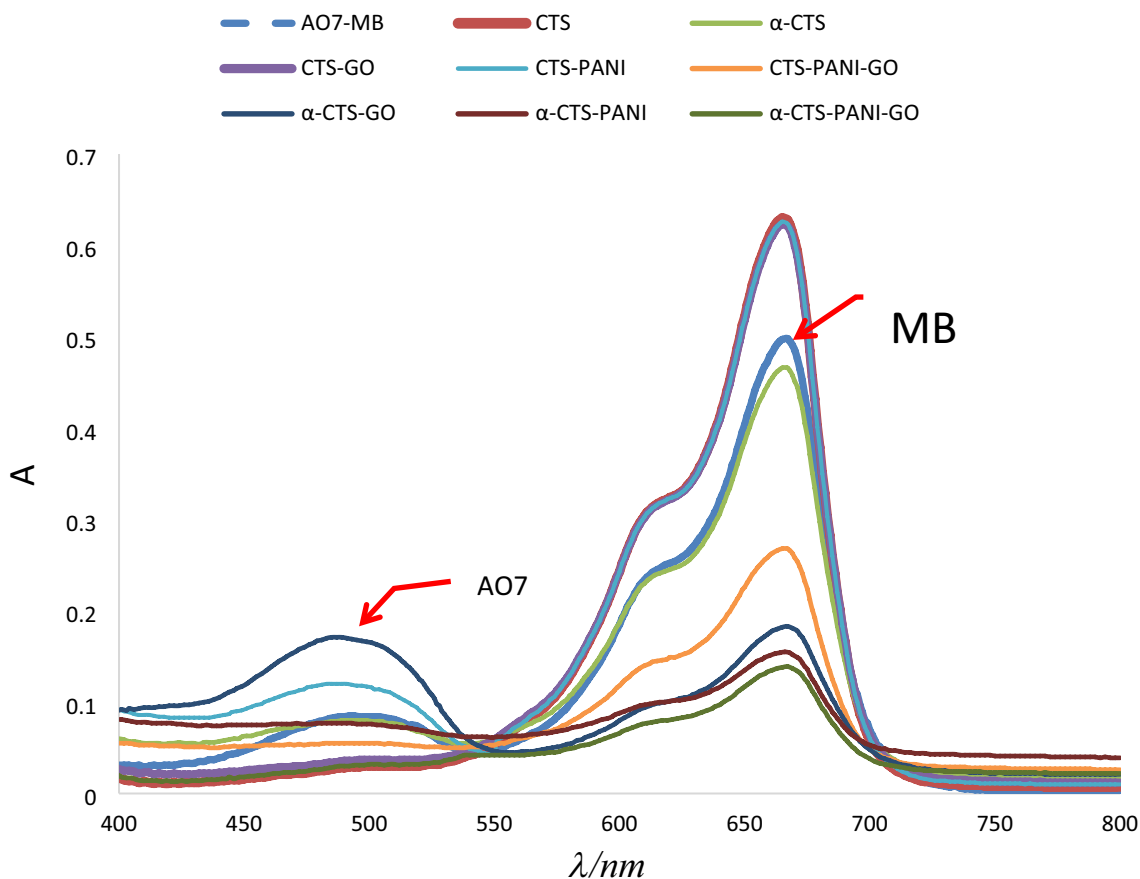**Fig. 15** The mechanism of the adsorbsion

Fig. 16 Comparison of UV–Visible spectrophotometer for, AO7-MB (**a**),CTS (**b**),CTS-GO (**c**), CTS-PANI (**d**), α-CTS (**e**), CTS-PANI-GO (**f**), α-CTS -GO (**g**), α-CTS-PANI (**h**), α-CTS-PANI-GO (**i**)

Table 3 Comparison of removal and adsorption percentage by different components

Component	Dye	adsorption capacity or removal rate	Reference
GO-PANI	alizarin red	58%	[61]
Chitosan-graphene oxide	Methylene Blue and Congo Red	201–152mg/g	[64]
chitosan/polyaniline nanofibrous	acid blue 113	814.9 mg/g	[62]
composite membranes	reactive orange	618.0 mg/g	[65]
graphene oxide/chitosan composite	methyl orange	271 mg/g	[63]
PANI/GO and PANI/RGO	Methylene blue	14.2 and	This work
α-CTS-PANI-GO	Methylene blue	19.2 mg g^{-1}	
	Acid Orange 7	80%	
		285 mg/g	
		95%	
		232 mg/g	

played a critical role during alizarin red adsorption on GO-PANI [61]. Also, according to the study by Liu et al., The as-prepared nanofibrous membranes exhibited significantly improved adsorption capacity of 814.9 and 618.0 mg/g towards acid blue 113 and reactive orange dyes, which were 121.8 and 99.4% higher than that of pure chitosan membrane [62]. Katowah et al. concluded that nanocomposite-based cross-linked PANI was created in the presence of hybrid nano-fillers mixed graphene oxide and single-walled carbon nanotubes (GO-OXS) doped CuO and coated with chitosan abbreviated as *C*–P (ANI-co-PPD)/Cs-GO-OXS/CuO NCs) is an effective adsorbent for the removal of hazardous dye from wastewater, which is both convenient and reusable [63].

Due to the effect of active sites, CTS and CTS-GO films have caused the adsorption of AO7 and its amount in the

solution has decreased. The adsorption rate of CTS and CTS-GO films did not differ in removing MB and in the presence of both films; the adsorption of MB in the solution has increased. This phenomenon is attributed to absorbing some of the available water by films that cause the increase of MB concentration in the solution. In the case of MB, the CTS-PANI film follows a similar manner to CTS and CTS-GO films. As well, in contrast to CTS and CTS-GO films, CTS-PANI film could not absorb AO7 dye, also. It may be due to the reduction of the activity of the CTS sites by the addition of PANI to the CTS film. As a result, the concentration of both dyes in the solution was increased with the adsorption of water by the CTS-PANI film. The α-CTS film showed an insignificant effect on the adsorption of AO7 and MB dyes. It indicated that the addition of α-ketoglutaric acid alone does not cause the adsorption of dyes. The α-CTS-GO film causes efficient adsorption of MB from the solution and shows more efficiency than the α-CTS and CTS-GO films. We were able to observe the synergistic effect of α-ketoglutaric acid and graphene oxide in the presence of each other. α-ketoglutaric acid endows the CTS film with more complexation ability and GO with negative charge endows the CTS film with stronger electrostatic interactions with cationic dyes.

The α-CTS-PANI film causes the effective removal of MB and it works much better than the α-CTS and CTS-PANI films. According to the previous information, the removal efficiency of CTS film for MB was increased significantly by the addition of PANI to the CTS film structure [19]. However, CTS-PANI, α-CTS-PANI, α-CTS films did not perform well in removing the AO7, probably the presence of PANI and α-ketoglutaric acid prevents the adsorption of AO7 by effective sites of chitosan. The CTS-PANI-GO film causes both MB and AO7 to be removed, while the CTS-GO and CTS-PANI films increased the concentration of MB by removing the AO7 and absorbing water. As it is clear in the adsorption diagram, according to our expectations, the addition of all three components (α-ketoglutaric acid, PANI, and GO) into the CTS film shows a perfect synergistic effect. The α-CTS-PANI-GO film revealed maximum adsorption capacity in comparison to all other films.

Conclusion

For the synthesis of the intended film, we used a cheap and biodegradable substrate. We also increased the adsorption percentage of target cationic and anionic pollutants of the synthetic flexible film by using graphene oxide and PANI, 80% for MB and 95% for AO7. We were able to prove, according to Fig. 16 that four substances, graphene oxide, PANI, Alpha-Ketoglutaric Acid, and CTS have a synergistic effect and increase the adsorption percentage and the value

of adsorbent capacity. Morphological analysis of FT-IR and Raman spectra showed that the intended pollutants were absorbed by the synthetic film. The adsorption of dye on the film was proved by the X-Ray diffraction analysis (XRD) method. According to the increase in the intensity of the peak before and after adsorption, it showed the presence of Methylene Blue (MB) and Acid Orange 7 (AO7). Also, the appearance of peaks related to sulfur in Energy dispersive X-ray (EDX) and EDX elemental mapping, and X-ray photoelectron spectroscopy (XPS) data after the adsorption process proved the presence of dye compounds and their adsorption by the synthetic film. Also, by studying the *point zero charge (pHpzc)* and the data obtained from the experimental design at a pH lower than 4.6, due to the positive charge of the film, the adsorption rate of anionic dye (AO7) was higher. At a pH higher than 4.6. The adsorption rate of cationic dye (MB) was higher. Also, high physical resistance and very easy separation of the synthetic film from the aqueous solution are notable features of this adsorbent. Also, this adsorbent showed a very good removal efficiency for the simultaneous removal of the mentioned cationic and anionic pollutants. In general, due to the importance of using hydrogels to remove pollutants from aquatic solutions, owing to its cost-effectiveness, ease of preparation and use, and high efficiency, it can be given a lot of attention in the future.

Declarations

Conflict of interest The authors have declared no conflict of interest.

References

1. Khalaf MN (2016) Green polymers and environmental pollution control. CRC Press
2. Khan I, Saeed K, Zekker I, Zhang B, Hendi AH, Ahmad A, Ahmad S, Zada N, Ahmad H, Shah LA (2022) Review on methylene blue: its properties, uses, toxicity and photodegradation. Water 14:242
3. Mahmoodi NM, Mokhtari-Shourijeh Z (2016) Preparation of aminated nanoporous nanofiber by solvent casting/porogen leaching technique and dye adsorption modeling. J Taiwan Inst Chem Eng 65:378–389
4. Mansoorian HJ, Bazrafshan E, Yari A, Alizadeh M (2014) Removal of azo dyes from aqueous solution using Fenton and

modified Fenton processes. Health Scope. https://doi.org/10.17795/jhealthscope-15507

5. Mahmoodi NM, Keshavarzi S, Ghezelbash M (2017) Synthesis of nanoparticle and modelling of its photocatalytic dye degradation ability from colored wastewater. J Environ Chem Eng 5:3684–3689

6. Silva JP, Sousa S, Rodrigues J, Antunes H, Porter JJ, Gonçalves I, Ferreira-Dias S (2004) Adsorption of acid orange 7 dye in aqueous solutions by spent brewery grains. Sep Purif Technol 40:309–315

7. Gupta V, Mittal A, Gajbe V, Mittal J (2006) Removal and recovery of the hazardous azo dye acid orange 7 through adsorption over waste materials: bottom ash and de-oiled soya. Ind Eng Chem Res 45:1446–1453

8. Hua Y, Xiao J, Zhang Q, Cui C, Wang C (2018) Facile synthesis of surface-functionalized magnetic nanocomposites for effectively selective adsorption of cationic dyes. Nanoscale Res Lett 13:1–9

9. Mostafazadeh N, Dadashi R, Faraji M, Bahram M, Koutamehr ME (2024) Anodizing of commercial galvanized mesh followed by electroless decorating of Ag nanoparticles for application as novel and low-cost photocatalyst for degradation of both dye and microbiological pollutants. J Photochem Photobiol A 447:115257

10. Crini G, Torri G, Lichtfouse E, Kyzas GZ, Wilson LD, Morin-Crini N (2019) Dye removal by biosorption using cross-linked chitosan-based hydrogels. Environ Chem Lett 17:1645–1666

11. Eze E, Omer AM, Hassanin AH, Eltaweil AS, El-Khouly ME (2023) Cellulose acetate nanofiber modified with polydopamine polymerized MOFs for efficient removal of noxious organic dyes. Environ Sci Pollut Res 620:333

12. Abu-Nada A, Abdala A, McKay G (2021) Removal of phenols and dyes from aqueous solutions using graphene and graphene composite adsorption: a review. J Environ Chem Eng 9:105858

13. Gohr MS, Abd-Elhamid A, El-Shanshory AA, Soliman HM (2022) Adsorption of cationic dyes onto chemically modified activated carbon: kinetics and thermodynamic study. J Mol Liq 346:118227

14. Jäger T, Mokos A, Prasianakis NI, Leyer S (2022) First_page settings order article reprints open accessarticle pore-level multiphase simulations of realistic distillation membranes for water desalination. Membranes 12:1112

15. Annadurai G, Ling LY, Lee J-F (2008) Adsorption of reactive dye from an aqueous solution by chitosan: isotherm, kinetic and thermodynamic analysis. J Hazard Mater 152:337–346

16. Sahariah P, Másson M (2017) Antimicrobial chitosan and chitosan derivatives: a review of the structure–activity relationship. Biomacromol 18:3846–3868

17. Derakhshi M, Naseri M, Vafaeipour Z, Malaekeh-Nikouei B, Jafarian AH, Ansari L (2023) Enhanced wound-healing efficacy of electrospun mesoporous hydroxyapatite nanoparticle-loaded chitosan nanofiber developed using pluronic F127. Int J Biol Macromol 240:124427

18. Vakili M, Rafatullah M, Salamatinia B, Abdullah AZ, Ibrahim MH, Tan KB, Gholami Z, Amouzgar P (2014) Application of chitosan and its derivatives as adsorbents for dye removal from water and wastewater: a review. Carbohyd Polym 113:115–130

19. Minisy IM, Salahuddin NA, Ayad MM (2021) Adsorption of methylene blue onto chitosan–montmorillonite/polyaniline nanocomposite. Appl Clay Sci 203:105993

20. Zhao Z, Huang Y, Wu Y, Li S, Yin H, Wang J (2021) α-ketoglutaric acid modified chitosan/polyacrylamide semi-interpenetrating polymer network hydrogel for removal of heavy metal ions. Colloids Surf, A 628:127262

21. Stejskal J, Gilbert R (2002) Polyaniline. Preparation of a conducting polymer (IUPAC technical report). Pure Appl Chem 74:857–867

22. An TNM, Phuc TT, Nhi DNT, Van Cuong N (2020) Removal of reactive red dye by reusable chitosan-polyaniline/Fe$_3$O$_4$ nanocomposite. Vietnam J Chem 58:477–481

23. Kadhim RJ, Al-Ani FH, Al-Shaeli M, Alsalhy QF, Figoli A (2020) Removal of dyes using graphene oxide (GO) mixed matrix membranes. Membranes 10:366

24. Junaidi N, Khalil N, Jahari A, Shaari N, Shahruddin M, Alias N, Othman N (2018) Effect of graphene oxide (GO) on the surface morphology & hydrophilicity of polyethersulfone (PES). IOP Conf Ser: Mater Sci Eng 358:012047

25. Yamazaki T, Chen S, Yu Y, Yan B, Haertlein TC, Carrasco MA, Tapia JC, Zhai B, Das R, Lalancette-Hebert M (2012) FUS-SMN protein interactions link the motor neuron diseases ALS and SMA. Cell Rep 2:799–806

26. Ali Khan M, Govindasamy R, Ahmad A, Siddiqui MR, Alshareef SA, Hakami AAH, Rafatullah M (2021) Carbon based polymeric nanocomposites for dye adsorption: synthesis, characterization, and application. Polymers 13:419

27. Nayl AA, Abd-Elhamid AI, Arafa WA, Ahmed IM, El-Shanshory AA, Abu-Saied MA, Soliman HM, Abdelgawad MA, Ali HM, Bräse S (2022) Chitosan-functionalized-graphene oxide (GO@CS) beads as an effective adsorbent to remove cationic dye from wastewater. Polymers 14:4236

28. Dadashi R, Bahram M, Faraji M (2022) Fabrication of a solid-state symmetrical supercapacitor based on polyaniline grafted multiwalled carbon nanotube deposit onto created vertically oriented graphene nanosheets on graphite sheet. J Energy Storage 52:104775

29. Chen J, Yao B, Li C, Shi G (2013) An improved Hummers method for eco-friendly synthesis of graphene oxide. Carbon 64:225–229

30. Pongener C, Bhomick PC, Supong A, Baruah M, Sinha UB, Sinha D (2018) Adsorption of fluoride onto activated carbon synthesized from *Manihot esculenta* biomass—equilibrium, kinetic and thermodynamic studies. J Environ Chem Eng 6:2382–2389

31. Zhou H, Hsu W-C, Duan H-S, Bob B, Yang W, Song T-B, Hsu C-J, Yang Y (2013) CZTS nanocrystals: a promising approach for next generation thin film photovoltaics. Energy Environ Sci 6:2822–2838

32. Elkomy MH, Ali AA, Eid HM (2022) Chitosan on the surface of nanoparticles for enhanced drug delivery: a comprehensive review. J Control Release 351:923–940

33. Ding P, Huang K-L, Li G-Y, Zeng W-W (2007) Mechanisms and kinetics of chelating reaction between novel chitosan derivatives and Zn (II). J Hazard Mater 146:58–64

34. Chen X, Wang X, Fang D (2020) A review on C1s XPS-spectra for some kinds of carbon materials. Fullerenes, Nanotubes, Carbon Nanostruct 28:1048–1058

35. Rouxhet P, Misselyn-Bauduin A, Ahimou F, Genet M, Adriaensen Y, Desille T, Bodson P, Deroanne C (2008) XPS analysis of food products: toward chemical functions and molecular compounds. Surf Interface Anal 40:718–724

36. Wang H, Skeldon P, Thompson G (1997) XPS studies of MoS$_2$ formation from ammonium tetrathiomolybdate solutions. Surf Coat Technol 91:200–207

37. Fukuda Y, Ichikawa S, Shimomura M, Sanada N, Suzuki Y (2002) Structures and electronic states of InAs (0 0 1) and (1 1 1) B surfaces passivated with sulfur studied by AES, LEED, UPS, XPS, and IPES. Vacuum 67:37–41

38. Zhang L, Hu P, Wang J, Huang R (2016) Crosslinked quaternized chitosan/bentonite composite for the removal of Amino black 10B from aqueous solutions. Int J Biol Macromol 93:217–225

39. Ngah WW, Hanafiah M, Yong S (2008) Adsorption of humic acid from aqueous solutions on crosslinked chitosan–epichlorohydrin beads: kinetics and isotherm studies. Colloids Surf B 65:18–24

40. Kumar N, Das S, Bernhard C, Varma GD (2013) Effect of graphene oxide doping on superconducting properties of bulk MgB_2. Supercond Sci Technol 26:095008

41. John A, Mahadeva SK, Kim J (2010) The preparation, characterization and actuation behavior of polyaniline and cellulose blended electro-active paper. Smart Mater Struct 19:045011

42. Queiroz MF, Teodosio Melo KR, Sabry DA, Sassaki GL, Rocha HAO (2014) Does the use of chitosan contribute to oxalate kidney stone formation? Mar Drugs 13:141–158

43. Minisy IM, Salahuddin NA, Ayad MM (2021) In vitro release study of ketoprofen-loaded chitosan/polyaniline nanofibers. Polym Bull 78:5609–5622

44. Haghighi Poudeh L, Letofsky-Papst I, Cebeci FÇ, Menceloglu Y, Yildiz M, Saner Okan B (2019) Facile synthesis of single-and multi-layer graphene/Mn_3O_4 integrated 3D urchin-shaped hybrid composite electrodes by core–shell electrospinning. ChemNanoMat 5:792–801

45. Perumbilavil S, Sankar P, Priya Rose T, Philip R (2015) White light Z-scan measurements of ultrafast optical nonlinearity in reduced graphene oxide nanosheets in the 400–700 nm region. Appl Phys Lett 107:051104

46. Jabbar A, Yasin G, Khan WQ, Anwar MY, Korai RM, Nizam MN, Muhyodin G (2017) Electrochemical deposition of nickel graphene composite coatings: effect of deposition temperature on its surface morphology and corrosion resistance. RSC Adv 7:31100–31109

47. Pasela BR, Castillo AP, Simon R, Pulido MT, Mana-Ay H, Abiquibil MR, Montecillo R, Thumanu K, Tumacder DV, Taaca KL (2019) Synthesis and characterization of acetic acid-doped polyaniline and polyaniline–chitosan composite. Biomimetics 4:15

48. Wang L, Yao Q, Bi H, Huang F, Wang Q, Chen L (2015) PANI/graphene nanocomposite films with high thermoelectric properties by enhanced molecular ordering. J Mater Chem A 3:7086–7092

49. Nirmala R, Il BW, Navamathavan R, El-Newehy MH, Kim HY (2011) Preparation and characterizations of anisotropic chitosan nanofibers via electrospinning. Macromol Res 19:345–350

50. Khalil WF, El-Sayyad GS, El Rouby WM, Sadek M, Farghali AA, El-Batal AI (2020) Graphene oxide-based nanocomposites (GO-chitosan and GO-EDTA) for outstanding antimicrobial potential against some Candida species and pathogenic bacteria. Int J Biol Macromol 164:1370–1383

51. Arjun N, Uma K, Pan G-T, Yang TC, Sharmila G (2018) One-pot synthesis of covalently functionalized reduced graphene oxide–polyaniline nanocomposite for supercapacitor applications. Clean Technol Environ Policy 20:2025–2035

52. Ederer J, Ecorchard P, Slušná MŠ, Tolasz J, Smržová D, Lupínková S, Janoš P (2022) A study of methylene blue dye interaction and adsorption by monolayer graphene oxide. Adsorpt Sci Technol. https://doi.org/10.1155/2022/7385541

53. El-Sharkaway E, Kamel RM, El-Sherbiny IM, Gharib SS (2019) Removal of methylene blue from aqueous solutions using polyaniline/graphene oxide or polyaniline/reduced graphene oxide composites. Environ Technol 41:2854

54. Huyen NTM, Trang PTT, Dat NM, Hieu NH (2017) Synthesis of chitosan/graphene oxide nanocomposites for methylene blue adsorption. AIP conference proceedings. AIP Publishing LLC, Melville, p 020013

55. Sabzevari M, Cree DE, Wilson LD (2018) Graphene oxide–chitosan composite material for treatment of a model dye effluent. ACS Omega 3:13045–13054

56. Sheshmani S, Ashori A, Hasanzadeh S (2014) Removal of acid orange 7 from aqueous solution using magnetic graphene/chitosan: a promising nano-adsorbent. Int J Biol Macromol 68:218–224

57. Garba ZN, Bello I, Galadima A, Lawal AY (2016) Optimization of adsorption conditions using central composite design for the removal of copper (II) and lead (II) by defatted papaya seed. Karbala Int J Modern Sci 2:20–28

58. Ho YS, McKay G (2000) The kinetics of sorption of divalent metal ions onto sphagnum moss peat. Water Res 34:735–742

59. Ben Amor I, Hemmami H, Laouini SE, Zeghoud S, Benzina M, Achour S, Naseef A, Alsalme A, Barhoum A (2023) Use of insect-derived chitosan for the removal of methylene blue dye from wastewater: process optimization using a central composite design. Materials 16:5049

60. Zeng W, Liu Y-G, Hu X-J, Liu S-B, Zeng G-M, Zheng B-H, Jiang L-H, Guo F-Y, Ding Y, Xu Y (2016) Decontamination of methylene blue from aqueous solution by magnetic chitosan ligno-sulfonate grafted with graphene oxide: effects of environmental conditions and surfactant. RSC Adv 6:19298–19307

61. Zhou J, Sun Y, Zhou C, Sun X, Han J (2023) Polyaniline/carbon hybrids: synthesis and application for alizarin red S removal from water. Colloids Surf, A 676:132204

62. Liu W, Lou T, Wang X (2023) Enhanced dye adsorption with conductive polyaniline doped chitosan nanofibrous membranes. Int J Biol Macromol 242:124711

63. Katowah DF, Saleh SM, Mohammed GI, Alkayal NS, Ali R, Hussein MA (2021) Ultra-efficient hybrid material-based cross-linked PANI@ Cs-GO-OXS/CuO for the photocatalytic degradation of Rhodamine-B. J Phys Chem Solids 157:110208

64. Pathirana MA, Dissanayake NS, Wanasekara ND, Mahltig B, Nandasiri GK (2023) Chitosan-graphene oxide dip-coated polyacrylonitrile-ethylenediamine electrospun nanofiber membrane for removal of the dye stuffs methylene blue and congo red. Nanomaterials 13:498

65. Pervez MN, Jahid MA, Mishu MMR, Talukder ME, Buonerba A, Jiang T, Liang Y, Tang S, Zhao Y, Dotto GL (2023) Tuning the surface functionality of polyethylene glycol-modified graphene oxide/chitosan composite for efficient removal of dye. Sci Rep 13:13460